[AMERICAN JOURNAL OF SCIENCE, VOL. 281, JANUARY, 1981, P. 1-34]

American Journal of Science

JANUARY 1981

LATE CENOZOIC RHYOLITES FROM THE KERN PLATEAU, SOUTHERN SIERRA NEVADA, CALIFORNIA

CHARLES R. BACON and WENDELL A. DUFFIELD

U.S. Geological Survey, 345 Middlefield Road,
Menlo Park, California 94025

ABSTRACT. Four late Cenozoic rhyolite domes lie atop the Kern Plateau, 30 to 40 km south-southeast of Mount Whitney. K-Ar and $^{40}Ar/^{39}Ar$ dating shows that Monache, Templeton, and Little Templeton Mountains are all about 2.4 m.y. old; a small dome nearby is approx 0.2 m.y. old. The three older rhyolites have SiO_2 = 73 to 74 percent and have steep, fractionated rare earth element (REE) patterns; the youngest has SiO_2 = 76 percent and a concave-upward REE pattern with a large negative Eu anomaly, Monache rhyolite contains the unusual phenocryst assemblage almandine + fayalite + biotite + oligoclase. The 2.4-m.y.-old rocks may be nearly unmodified partial melts of crustal sources, whereas the 0.2-m.y.-old rhyolite may be a product of relatively shallow differentiation. The rhyolites and nearby basalts are coeval with mafic and silicic volcanic rocks in the Coso Range about 40 km to the southeast. Their generation and eruption may reflect intense tectonic extension at the margin of the Basin and Range province and concomitant relaxation of compressive stress in a west-northwest direction, allowing melts to reach the surface in the adjacent Sierra Nevada.

INTRODUCTION

Four rhyolite domes of late Cenozoic age occur in the southern Sierra Nevada between the Kern River Canyon and Olancha Peak. Of these, Monache, Templeton, and Little Templeton Mountains have yielded K-Ar and $^{40}Ar/^{39}Ar$ ages of approx 2.4 m.y. and lie in broad, alluviated valleys. The fourth dome is much younger, with a K-Ar age of about 0.2 m.y., is more silicic, and was extruded at the head of Long Canyon (figs. 1 and 2).

Lawson (1904, p. 321) viewed Templeton Mountain from a distance and recognized it as an extinct volcano. Knopf (1918, p. 73) visited both Templeton and Monache Mountains and remarked that both were composed of somewhat similar glassy lava, which he provisionally called latite. A more detailed description of the Monache and Templeton occurrences, as well as basalt flows to the north and west (fig. 2), was given by Webb (1946, 1950), who proposed that the highly symmetrical cones of Monache and Templeton were eroded volcanic domes of similar age. Mayo (1947, p. 499) briefly alluded to Templeton, Monache, and the Long Canyon dome but failed to recognize the relative youth or highly silicic character of the last. The Pleistocene age of the Long Canyon dome was first noted by Wood (1977, p. 49), who rediscovered the locality by tracing exposures of pumice in stream banks and suggested that the source of these deposits might be as young as 30,000 to 100,000 years old.

In this paper we present new analytical data on rocks from all four domes, including rapid-rock and instrumental neutron activation analyses, electron microprobe analyses of minerals, and K-Ar and $^{40}Ar/^{39}Ar$

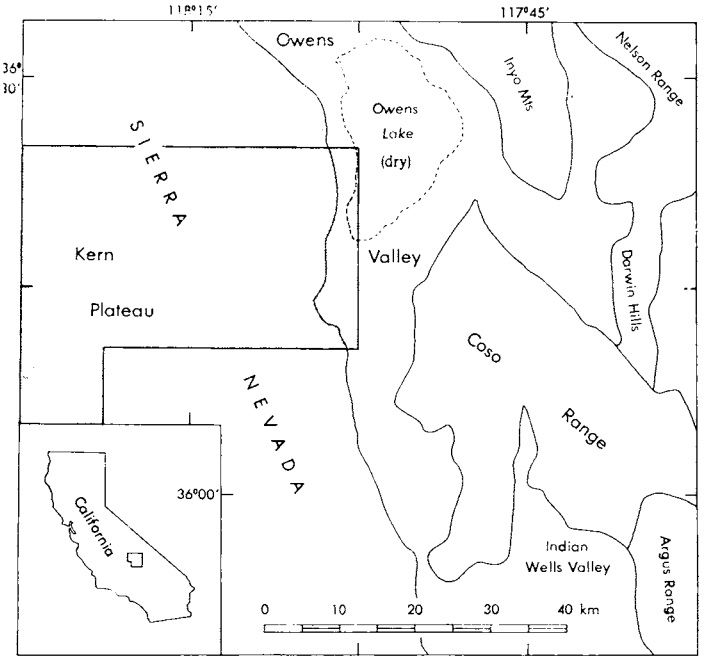

Fig. 1. Map showing location of area of fig. 2 (shaded) with respect to Coso Range and southern Owens Valley.

TABLE 1

Calculated ages and analytical data for K and Ar

$^{40}Ar/^{39}Ar$ total fusion analyses*

Sample number	Material	$^{40}Ar/^{39}Ar$	$^{37}Ar/^{39}Ar$	$^{38}Ar/^{39}Ar$	% $^{39}Ar_{Ca}$	% $^{39}Ar_{K}$	% $^{40}Ar_{rad}$	Calculated age (10^6 yrs)
M-3	Biotite	1.100	0.00260	0.00291	0.02	0.5	21.4	2.42 ± 0.12
T-1	Biotite	2.620	0.0205	0.00805	0.07	0.2	9.0	2.44 ± 0.26

K-Ar analytical data

Sample number	Material	K_2O**	Weight (g)	$^{40}Ar_{rad}$ (mol/g)	$\frac{100\ ^{40}Ar_{rad}}{^{40}Ar\ total}$	Calculated age*** 10^6 yrs
T-2	Biotite	8.25	1.652	28.37×10^{-12}	5.9	2.39 ± 0.12
LC-1	Sanidine	9.45	8.886	2.653	36.6	0.185 ± 0.015
			8.644	2.408	17.8	

* Isotope ratios are as measured after correcting for instrumental factors, except ^{37}Ar has been corrected for decay (half-life = 35.1 days). Subscripts Ca, K, and rad refer to calcium-derived, potassium-derived, and radiogenic argon, respectively. J = 0.00571.

** Mean of two measurements.

*** $\lambda_\epsilon = 0.581 \times 10^{-10}yr^{-1}$, $\lambda_\beta = 4.693 \times 10^{-10}yr^{-1}$, $^{40}K/K = 1.167 \times 10^{-4}$ mol/mol. Errors are estimated standard deviations (Cox and Dalrymple, 1967). Where more than one measurement was made, the calculated age is a weighted mean, where weighting is by inverse of the variance of the individual measurement.

age determinations. In addition, $^{87}Sr/^{86}Sr$ ratios have been obtained for samples from Templeton and Monache Mountains. These data are used to decipher the petrogenesis of the rhyolites and relate them to other late Cenozoic volcanic rocks nearby. The significance of these silicic volcanoes to the geothermal potential of the southern Sierra Nevada is briefly discussed.

AGE AND VOLUME

The conical forms of both Templeton and Little Templeton Mountains and the presence of glassy rock in places on their surfaces suggest that they are volcanic domes that have been little modified by erosion since their formation. However, sufficient time has elapsed for removal of pyroclastic material and exposure of partly devitrified rocks. Templeton Mountain rises 405 m above the surrounding meadows, has an average basal diameter of about 2900 m, and a volume of about 0.9 km^3. The smaller dome, Little Templeton Mountain, is 150 m high, about 1100 m in diameter, and has a volume of approx 0.05 km^3. We have found no field evidence as to which mass is the older of the two.

Samples of porphyritic hydrated glass were obtained from near the summits of both Templeton domes (table 1 and fig. 2). Only a small amount of biotite was recovered from sample T-1 (Templeton Mountain), necessitating age determination by the $^{40}Ar/^{39}Ar$ method. The samples have calculated ages that are indistinguishable: 2.44 ± 0.26 m.y. (T-1) and 2.39 ± 0.12 m.y. (T-2) (table 1). These results are considered reasonable in light of the geomorphic setting of the domes.

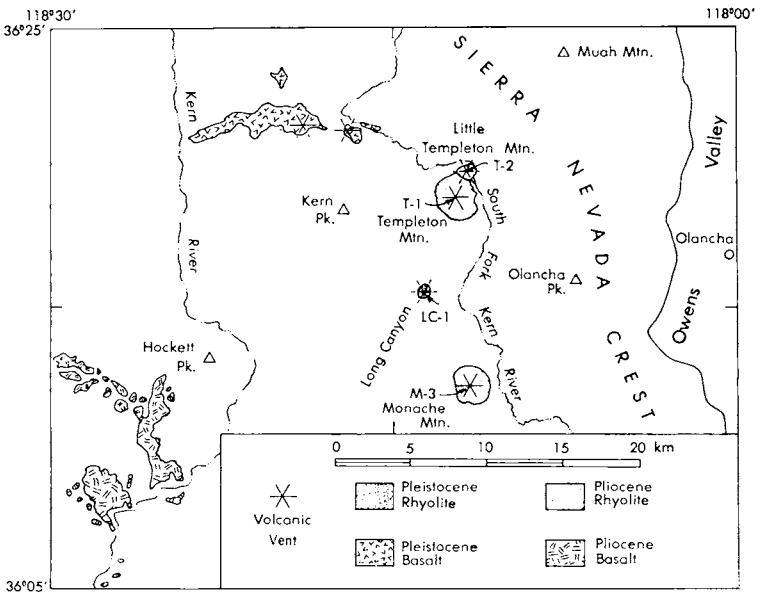

Fig. 2. Sketch map showing late Cenozoic volcanic rocks and some physiographic features of part of the southern Sierra Nevada (modified after Matthews and Burnett, 1965, and Moore and du Bray, 1978).

Monache Mountain attains a height of 460 m, with an average basal diameter of around 2600 m. Its calculated volume is 0.9 km³. The similarity in size, shape, degree of erosion, and setting between Templeton and Monache Mountains invites the inference that they are of similar age and origin.

The freshest material from the Monache dome consisted of spheroidal blocks of fresh, black prophyritic rock up to about 25 cm in longest dimension that had apparently weathered out of partly devitrified, hydrated glass. The small amount of biotite that was recovered from this sample was analyzed by the $^{40}Ar/^{39}Ar$ method, yielding a calculated age of 2.42 ± 0.12 m.y. (table 1, M-3), supporting the idea of essentially contemporaneous eruption of rhyolite at the Templeton and Monache centers.

The relative youth of the Long Canyon eruptive center was recognized by Wood (1977, p. 49), who noted that the valley downstream has aggraded 5 to 10 m with fine ash and lapilli eroded from the tephra ring that partly surrounds the dome. The flat-topped dome is 100 m

TABLE 2

Major-element analyses and CIPW norms
(calculated on an anhydrous basis)

	M-3	T-1	T-2	LC-1	LC-1g
SiO_2	73.1	72.1	72.6	76.6	75.9
Al_2O_3	15.2	14.2	14.2	13.3	13.0
Fe_2O_3	0.74	0.69	1.0	0.25	—
FeO	1.3	0.96	0.72	0.24	0.46*
MgO	0.05	0.27	0.10	0.02	0.02
CaO	0.61	1.3	0.81	0.59	0.36
Na_2O	4.8	4.1	4.1	4.0	3.94
K_2O	4.4	3.5	4.3	4.4	5.08
H_2O+	0.15	1.9	1.1	1.3	—
H_2O-	0.05	0.10	0.90	0.23	—
TiO_2	0.03	0.26	0.06	0.06	0.05
P_2O_5	0.03	0.05	0.03	0.02	—
MnO	0.07	0.04	0.05	0.10	0.13
CO_2	0.02	0.01	0.02	0.01	0.6**
Total	100.55	99.48	99.99	101.12	99.29***
SiO_2†	72.8	74.0	74.1	76.9	76.4
Fe/Fe + Mg	0.98	0.88	0.95	0.97	0.97
CIPW Norms, weight percent					
Q	26.16	32.27	30.95	35.28	32.90
C	1.55	1.48	1.48	0.96	0.37
or	25.91	21.22	25.93	26.11	30.33
ab	40.48	35.59	35.41	33.99	33.68
an	2.69	6.22	3.77	2.74	1.80
hy	1.97	1.55	0.75	0.37	0.45
mt	1.07	1.03	1.48	0.36	0.37
il	0.06	0.51	0.12	0.11	0.10
ap	0.07	0.12	0.07	0.05	—
cc	0.05	0.02	0.05	0.02	—

SiO_2† is the silica content calculated H_2O-free, with the analysis normalized to total 100.00.

Analyses by method described under "single solution" in Shapiro (1975); F. Brown and H. Smith, analysts, U.S. Geol. Survey, Reston, Va. LC-1g microprobe analysis of glass; * Fe as FeO; * * F, omitted from norm calculation; * * * less 0.25 O for F.

high, has an estimated basal diameter of 900 m, upper diameter of 700 m, and calculated volume of approx 0.05 km^3. Wood (1977) states that the tephra ring is eroded to about the same extent as nearby early Wisconsin moraines and that bombs 1 m in diameter can be found on top of the adjacent Kingfisher ridge (0.6 km). The dome blocked the path of the stream, which incised it and exposed its devitrified core. Local exposures of the original highly prophyritic, glassy carapace remain, some containing blocks with millimeter-size bits of fresh glass in a matrix of crystal-rich, hydrated glass. Sample LC-1 was obtained from the cores of several of these blocks (fig. 2). The conventional K-Ar sanidine age is well constrained at 0.185 ± 0.015 m.y. (table 1) and is within a factor of two of Wood's (1977) estimate of the age of the associated tephra ring.

CHEMISTRY

Major Elements

Chemical analyses of fresh rock from each of the four Sierra Nevada volcanic domes are presented in table 2, along with CIPW norms calculated on an anhydrous basis. All of these samples are corundum-normative rhyolites with high Fe/(Fe+Mg). The peraluminous character of the perlitic rocks (T-1, T-2, LC-1) may be due to a slight loss of Na during the process of hydration.

The sample from Monache Mountain (table 2, M-3) possesses a number of unusual features. For a fresh volcanic rock that contains about 73 percent SiO_2, it is particularly rich in Al_2O_3 and total Fe and poor in MgO, CaO, and TiO_2. These peculiarities become less pronounced when M-3 is compared with analyses of LC-1 (table 2) and of late Cenozoic high-silica (> 75 percent SiO_2) rhyolites from east of the Sierra Nevada in the Coso Mountains (Duffield, Bacon, and Dalrymple, 1980 and unpub. data), at Mono Craters (Carmichael, 1967), Long Valley (Noble and others, 1972), and near Big Pine (R. L. Smith, unpub. data). Loss of Si or addition of a small amount of material rich in Al and Fe relative to Si to any one of these high-silica rhyolites, with adjustment of Na/K, would produce a rock very like the rhyolite of Monache Mountain in major-element chemistry. Alternatively, M-3 might be viewed as a more differentiated, relatively sodic and aluminous version of T-2.

The analyses of the two samples from the Templeton center (table 2, T-1, T-2) are grossly similar, both having nearly identical SiO_2, Al_2O_3, total Fe, MnO, and Na_2O contents. The main mass of Templeton Mountain (T-1) is richer in MgO, CaO, TiO_2, and P_2O_5 and poorer in K_2O than Little Templeton Mountain. Most of the reported H_2O must be meteoric, introduced by the process of hydration of volcanic glass (Friedman and Smith, 1955). T-1 is compositionally similar to some of the silicic rocks of the Mount Lassen and Inyo Craters areas (Carmichael, 1967).

The sample from the Long Canyon dome is a high-silica rhyolite (table 2, LC-1). The hydration of some of the glass has resulted in a value for H_2O intermediate between obsidians and perlites (Ross and

Smith, 1955). It is very like other late Cenozoic high-silica rhyolites from the Western United States in many respects, being very poor in MgO, TiO_2, and P_2O_5. This sample and its residual glass (table 2, LC-1g) have relatively low total Fe and high Al_2O_3 and, particularly, MnO contents. However, in the overall context of volcanic rocks, these differences are subtle.

Trace Elements

The same four samples that were analyzed for major elements were analyzed for 23 trace elements and Fe by instrumental neutron activation (INAA). The INAA data are presented in table 3 and supplemented by the Rb and Sr values by high-precision X-Ray fluorescence (XRF) in table 4.

The trace-element contents of the Pliocene rhyolites are grossly similar yet contrast greatly with those of the Pleistocene rhyolite (LC-1). Of the three Pliocene domes, those of the Templeton center are most likely related to each other. The sample from the more voluminous of the two (Templeton Mountain), T-1, appears to be the less differentiated, both with respect to trace as well as major elements. It is richer in Sc, Cr, Co, Zr, Ba, Eu, and Hf, whereas T-2 is relatively enriched in

TABLE 3

Instrumental neutron activation analyses. All values in ppm except for Fe.

	σ, percent**	M-3	T-1	T-2	LC-1
Sc	1	2.25	2.32	1.69	5.42
Cr	45	2.1	<3.5	1.4	<2.5
Fe, percent	1	1.61	1.31	1.38	0.43
Co	35	0.2	1.1	0.3	0.3
Zn	4	73	48	62	42
Rb	4	120	69	102	288
Zr	13	200	240	160	130*
Sb	27	0.7	<1.0	0.4	3.4
Cs	6	1.9	1.2	1.7	12.1
Ba	1	1270	2230	1480	<120
La	2	61	48	53	12
Ce	2	108	77	92	24
Nd	6	37	29	31	10*
Sm	1	6.2	4.7	5.4	1.3*
Eu	1	0.84	0.96	0.81	0.10
Tb	10	0.66	0.41	0.50	0.45
Tm	15	0.26	0.20	0.26	<0.45
Yb	5	2.3	1.4	1.8	3.1
Lu	5	0.32	0.22	0.27	0.54
Hf	2	5.2	4.9	4.2	4.0
Ta	9	1.46	0.76	1.14	3.98
Th	2	9.4	6.0	7.7	26.3
U	6	2.4	1.7	2.3	13.8
La/Sm		9.8	10.2	9.8	9.2
La/Yb		26.5	34.3	29.4	3.9
Th/U		3.9	3.5	3.3	1.9

< Indicates that abundance is less than reported (background) value.
* Correction for fission product interference exceeds 20 percent of reported value.
** Error limits are one standard deviation based on counting statistics alone.
Analyses by P. A. Baedecker, U.S. Geol. Survey, Reston, Va.

TABLE 4
Rb, Sr, and $^{87}Sr/^{86}Sr$

	M-3	T-1
Rb, ppm	125	74
Sr, ppm	115	401
Rb/Sr	1.09	0.185
$^{87}Sr/^{86}Sr$	0.70593 ± 0.00028	0.70638 ± 0.00018

Rb and Sr abundances by X-ray fluorescene, U.S. Geol. Survey, Reston, Va.; J. R. Lindsay and J. B. McCall, analysts.

$^{87}Sr/^{86}Sr$ normalized to $^{86}Sr/^{88}Sr = 0.1194$ and E. and A. $SrCO_3$ $^{87}Sr/^{86}Sr = 0.7080$, U.S. Geol. Survey, Menlo Park, Calif.; A. C. Robinson, analyst.

Zn, Rb, Cs, Ta, Th, U, and rare earth elements (REE) other than Eu. In addition, the concentrations of Zr, Ba, and Sr are notably high in T-1 (Jack and Carmichael, 1968; Dodge, 1972).

The sample from Monache Mountain (M-3) appears, on the basis of trace-element composition, to be more closely related to the rocks from the Templeton center than to high-silica rhyolites, such as the rhyolite of Long Canyon (LC-1). The concentrations of trace elements in the Monache rhyolite suggest that it is comparable to the rhyolite of Little Templeton Mountain, though richer in Fe, Mn, and Al and perhaps slightly more evolved, and that the same general physical processes have governed the differentiation history of these rocks.

The rhyolite of Long Canyon (LC-1) displays trace-element compositional characteristics similar to the other high-silica rhyolites previously mentioned. It appears to be more highly evolved than the high-silica rhyolites of Long Valley (Noble and others, 1972; Hildreth, ms) but less so than those of the nearby Coso Mountains (Bacon, Macdonald, Duffield, Smith, and Baedecker, unpub. data). Compared to the samples from the Monache and Templeton centers, LC-1 is enriched in Sc, Rb, Sb, Cs, Yb, Lu, Ta, Th, and U and depleted in Zn, Sr, Zr, Ba, light REE, and Eu.[1] These differences are also apparent in certain elemental ratios: La/Sm is similar in both, but La/Yb is almost an order of magnitude lower in LC-1; Th/U is also considerably lower (1.9) in LC-1 than the more "normal" values of 3.3 to 3.9 for the Pliocene rhyolites.

The concentrations of the REE determined in this study, normalized to chondritic abundances, are plotted in figure 3. T-1 has the lowest REE abundances of the three Pliocene rhyolites and shows no Eu anomaly. T-2 is more fractionated, with a noticeable negative Eu anomaly, whereas M-3 is more fractionated still. LC-1 shows a steep light REE pattern, high La/Sm, though with much lower concentrations, a large negative Eu anomaly, and high heavy REE contents (low La/Yb). This pattern of REE abundances falls within the range of REE patterns for other high-silica rhyolites, some leucogranites, and aplites and suggests that similar processes have contributed to the formation of such magmas.

[1] Note added in proof: Emission spectrographic analysis of LC-1 yields Sr = 21 ppm and Ba = 26 ppm.

Sr ISOTOPES

The isotopic composition of Sr has been determined for the samples from Monache (M-3) and Templeton Mountains (T-1). The ratios $^{87}Sr/^{86}Sr$, Rb/Sr, and the concentrations of Rb and Sr are given in table 4.

Kristler and Peterman (1973) demonstrated the existence of systematic areal variation of initial $^{87}Sr/^{86}Sr$ in the Sierra Nevada independent of the age of granitic rocks and coincident with initial $^{87}Sr/^{86}Sr$ in superjacent late Cenozoic mafic and intermediate volcanic rocks. $^{87}Sr/^{86}Sr$ values for the rhyolites of Monache and Templeton Mountains, 0.7059 and 0.7064, are consistent with this pattern.

Rb and Sr concentrations determined for sample T-1 (table 4) are within the range given by Kristler and Peterman (1973) for Sierra Nevada granitic rocks. Rb/Sr is unusually high in sample M-3, and the Sr content is low relative to other igneous rocks of similar SiO_2 content. These parameters approach values typical of rhyolites of significantly higher SiO_2 content, such as some of the later ash flows of the Bishop Tuff (Hildreth, 1979, table 2).

The Sr isotope data appear to rule out metasedimentary sources for either M-3 or T-1, on the basis of the data of Kistler and Peterman (1973, table 2). The isotopic data are consistent with low-Rb sources within the Sierra Nevada basement or with deeper, perhaps more mafic,

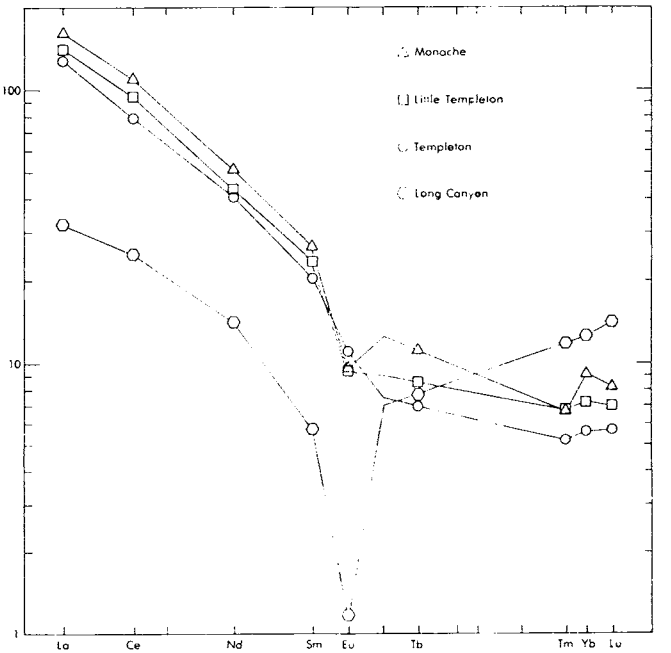

Fig. 3. REE abundances for Sierra Nevada rhyolites, normalized to values for Leedey chondrite (Masuda, Nakamura, and Tanaka, 1973), and plotted as function of ionic radius.

sources. The low Sr content of M-3 and its $^{87}Sr/^{86}Sr$ ratio of 0.7059 suggest that material with high $^{87}Sr/^{86}Sr$ did not contribute significantly to the Monache magma, even if the low Sr content was brought about by later extensive fractionation of a phase with low Rb/Sr. Rb/Sr for M-3 suggests a metasedimentary or highly differentiated igneous source, or, alternatively, a relatively small degree of partial melting of material with significantly lower Rb/Sr. Some granitic rocks in Australia with relatively high Rb/Sr and low initial $^{87}Sr/^{86}Sr$ are thought to have been derived from young pelitic metasedimentary sources (Flood and Shaw, 1977). A whole-rock $\delta^{18}O$ value of $+7.8 \pm 0.1$ per mil (J. R. O'Neil, personal commun., 1978) and other evidence presented later is inconsistent with such an hypothesis for the source of the Monache magma.

MINERALOGY

Microscopic examination of thin sections and chemical analysis of minerals provide the basis for interpretation of the cooling and crystallization histories of the Kern Plateau rhyolites. The assemblages of phenocryst phases in the rocks and the compositions of the minerals reflect also the chemical compositions of the magmas and possibly their source regions.

Electron Microprobe Analytical Techniques

All major phenocryst phases, some accessory phases, and a residual glass were analyzed by the first author with the ARL-EMX microprobe at the U.S. Geological Survey in Menlo Park, Calif. Data were collected at an accelerating voltage of 15 kv, with counting terminated at constant total beam current, and reduced with the ZAF correction program FRAME (Yakowitz, Myklebust, and Heinrich, 1973). All elements were determined with wavelength-dispersive spectrometers except Si, P, Ca, and Fe in apatite and Al, Si, and Fe in feldspars, which were determined with an energy-dispersive system. The latter were monitored primarily for use in the matrix correction program. The feldspar analytical data are presented in graphical form only (fig. 4). A variety of natural and synthetic mineral standards was employed.

Rhyolite of Templeton Mountain

The rhyolite of Templeton Mountain (for example T-1) contains euhedral, faintly oscillatory-zoned plagioclase crystals up to 3 mm long as the dominant phenocryst phase (table 5). These carry small inclusions of magnetite, ilmenite, apatite, biotite, hornblende, hypersthene, zircon, and colorless glass. The most calcic plagioclase ($An_{54.1}Ab_{44.6}Or_{1.3}$, fig. 4A) is a small, rounded core zone, which may represent a xenocryst or residual material from the magma source. Most phenocryst compositions, however, lie between $An_{38.3}Ab_{59.4}Or_{2.3}$ and $An_{24.6}Ab_{71.8}Or_{3.6}$. Enhedral plagioclase microphenocrysts (<0.2 mm) form a second population with thin, relatively calcic margins and cores that are slightly more sodic than phenocryst rims (fig. 4A). Plagioclase also occurs in all sizes from small microphenocrysts to microlites.

Euhedral, green to brown pleochroic hornblende phenocrysts up to 3 mm long define a strong lineation, are commonly intergrown with plagioclase and Fe–Ti oxide phenocrysts, are somewhat inhomogeneous, and are subtly zoned toward more Fe-rich and Mg- and Ti-poor rims. Rare inclusions of apatite and Fe–Ti oxides are present. Small needles of an optically similar amphibole grade downward in size through microphenocrysts to microlites in the groundmass.

Brown euhedral biotite phenocrysts form flakes up to 1 mm in diameter. Similar to hornblende, biotite phenocrysts have rims that are slightly richer in Fe and poorer in Mg and Ti than the cores. Biotite phenocrysts contain tiny needles of apatite and rare glass inclusions. Biotite is far more abundant as microphenocrysts (table 5) and persists into the groundmass.

Pink to green pleochroic, euhedral hypersthene up to 1 mm long is a rare phenocryst phase, most commonly found intergrown with plagioclase phenocrysts. The hypersthene crystals contain Fe–Ti oxide and apatite microphenocrysts as inclusions. They are considerably richer in Mn than the associated biotite and hornblende (table 6).

Both ulvospinel–magnetite and ilmenite–hematite solid solutions, hereafter referred to as magnetite and ilmenite, are present as euhedral phenocrysts up to about 0.4 mm in diameter. The phenocrysts are homogeneous and poor in Ti (table 7) relative to those from rocks of similar SiO_2 content analyzed by Carmichael (1967). Inclusions of apatite are

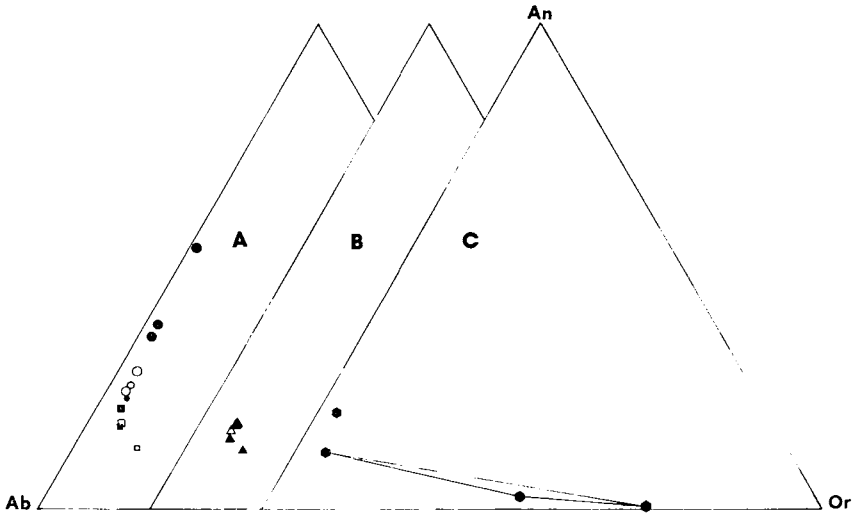

Fig. 4. Compositions of feldspars determined by electron microprobe plotted on molecular An–Ab–Or diagrams. Symbols same as figure 2; filled symbols represent average cores, open symbols rims; large symbols are phenocrysts, small groundmass. (A) Templeton domes. Note continuation of trend established by T-1 in T-2 feldspars. Most calcic plagioclase is single phenocryst core that may be restite. (B) Rhyolite of Monache Mountain. (C) Rhyolite of Long Canyon. Tie lines connect phenocrysts and normative composition of glass (open hexagon; table 2). More calcic plagioclase is single phenocryst core.

common in both phases. One bleb of pyrrhotite, presumably representing quenched, immiscible sulfide liquid, was found in an ilmenite phenocryst. The bulk of subphenocryst-size oxide crystals consists of groundmass magnetite poorer in Mg, Al, Ti, and V and richer in Fe^{3+} and Mn than the phenocrysts.

Euhedral microphenocrysts of colorless apatite and zircon about 0.1 mm long occur rarely in the groundmass of microlites and colorless glass.

Rhyolite of Little Templeton Mountain

The compositional trend of phenocryst precipitation evident in the rhyolite of Templeton Mountain is continued in the rhyolite of Little Templeton Mountain (T-2). This trend is most clearly shown by plagioclase, which forms euhedral, faintly oscillatory-zoned phenocrysts as large as 3 mm and abundant euhedral microphenocrysts 0.2 mm and smaller. Plagioclase phenocrysts contain inclusions of biotite, apatite, zircon, and colorless glass. Cores of phenocrysts are slightly more sodic than cores of microphenocrysts of T-1 (fig. 4A). Cores of normally zoned microphenocrysts from T-2 overlap rims of phenocrysts in composition. Feldspar is also present in the glassy groundmass as microlites.

Phenocrysts of brown biotite in T-2 are euhedral plates up to 2.5 mm in diameter. Preferred orientation of these crystals gives the rock a foliated appearance. Biotites are unzoned, except with respect to F, which decreases toward the margins. They are richer in Al, Fe, K, and Mn and poorer in Si, Mg, Ti, and F than biotite phenocrysts in T-1

TABLE 5

Modal analyses of representative thin sections based on a total of 1000 points counted on each section (volume percent), supplemented by examination of mineral separations

	M-3	T-1	T-2	LC-1
Phenocrysts				
Quartz	—	—	—	6
Sanidine	—	—	—	9
Plagioclase	2	4	5	5
Biotite	0.6	tr.	1	tr.
Hornblende	—	0.3	—	—
Hypersthene	—	tr.	—	—
Fayalite	tr.	—	—	—
Garnet	tr.	—	—	—
Microphenocrysts				
Plagioclase	8	10	21	—
Biotite	0.7	2	5	tr.
Hornblende	—	0.3	—	—
Hypersthene	—	tr.	—	—
Fayalite	0.7	—	—	—
Zircon	tr.	tr.	tr.	—
Magnetite	—	0.1	tr.	tr.
Ilmenite	—	0.1	—	tr.
Apatite	tr.	tr.	tr.	tr.
Groundmass	88	83	68	80

Tr., trace.

(table 6). Colorless glass and tiny needles of apatite (?) are the only inclusions. The size of biotite crystals grades continuously from phenocrysts to microlites.

The only Fe–Ti oxide phase found in T-2 is magnetite. Very small crystals are abundant in the glassy groundmass; extremely rare phenocrysts of magnetite occur intergrown with or attached to biotite. The largest phenocrysts are about 0.2 mm in diameter, euhedral, unzoned, and, surprisingly, richer in Ti than magnetite microphenocrysts from T-1. They also have higher Si, Al, and Mn and lower Mg, Zn, and especially V contents than T-1 magnetites (table 7).

The groundmass of T-2 consists of colorless glass and microlites. Prismatic microphenocrysts of zircon 0.1 mm long are extremely rare.

Three fragments of unzoned augite were found in a heavy-mineral concentrate from T-2. Their compositions are similar to augites from rocks of similar or slightly lower SiO_2 content analyzed by Carmichael (1967), but the small, compositionally heterogeneous population implies that they were not in equilibrium with other phases that make up the phenocryst assemblage.

TABLE 6

Representative microprobe analyses of ferromagnesian silicates

	M-3	M-3	M-3	T-1	T-2	LC-1	T-1	T-1
	Fayalite	Garnet	Biotite	Biotite	Biotite	Biotite	Hornblende	Hypersthene
SiO_2	31.0	37.4	34.1	37.2	34.4	37.9	42.8	51.1
Al_2O_3	0.00	20.3	15.7	14.9	15.8	13.3	10.2	1.32
FeO*	64.8	32.3	33.1	20.2	29.7	21.7	17.2	28.0
MgO	2.76	1.23	3.30	11.3	4.46	10.3	12.2	18.2
CaO	0.09	4.53	0.01	0.03	0.01	0.00	10.1	0.70
MnO	2.92	5.01	0.38	0.16	0.29	1.88	0.37	1.21
TiO_2	0.02	0.16	2.39	4.50	3.72	3.62	2.00	0.12
Na_2O	0.02	0.04	0.59	0.71	0.58	0.45	2.11	0.04
K_2O	—	—	8.68	8.21	8.68	9.53	0.60	—
F	—	—	0.19	0.55	0.18	1.1	0.17	—
less O	—	—	0.08	0.23	0.08	0.46	0.07	—
H_2O**	—	—	3.69	3.75	3.73	3.47	1.92	—
Total	101.61	100.97	102.05	101.28	101.47	102.79	99.60	100.69
				Formulae				
Si	1.009	6.028	2.706	2.777	2.700	2.848	6.433	1.952
Al	0.000	3.856	1.469	1.311	1.462	1.178	1.807	0.059
Fe	1.763	4.354	2.197	1.261	1.950	1.364	2.162	0.895
Mg	0.134	0.295	0.390	1.258	0.522	1.154	2.733	1.036
Ca	0.003	0.782	0.001	0.002	0.001	0.000	1.627	0.029
Mn	0.080	0.684	0.026	0.010	0.019	0.120	0.047	0.039
Ti	0.001	0.020	0.143	0.253	0.220	0.205	0.226	0.003
Na	0.002	0.012	0.091	0.103	0.089	0.066	0.615	0.003
K	—	—	0.878	0.782	0.869	0.914	0.115	—
F	—	—	0.048	0.130	0.045	0.261	0.081	—
OH**	—	—	1.952	1.870	1.955	1.739	1.919	—
anions	4	24	12	12	12	12	24	6

* Total Fe as FeO.

** H_2O calculated assuming full hydroxyl site occupancy and no ferric iron, with OH equal to 2-F.

Analyses are averages of several crystals, excluding rims.

Rhyolite of Monache Mountain

The rhyolite of Monache Mountain (sample M-3) is not only unusual in chemical composition but sports a bizarre assemblage of phenocrysts as well. Plagioclase and biotite are fairly abundant and are accompanied by very rare, but conspicuous, red garnet and yellow fayalite. No Fe–Ti oxide phenocrysts or microphenocrysts are present; only Ti-poor magnetite has been found as tiny crystals in the groundmass.

Plagioclase phenocrysts are up to 4 mm long, euhedral, faintly oscillatory-zoned, and of fairly uniform composition (fig. 4B). They contain inclusions of zircon, apatite, fayalite, biotite, and colorless glass. Microphenocrysts cores are more potassic than phenocrysts, yet these crystals are zoned toward the phenocryst compositions (fig. 4B).

Deep greenish-brown euhedral plates of biotite as large as 2 mm make up less than 1 percent of the rock and are very rich in Fe (table 6), as one would expect from a rock with abundant fayalite and high Fe/(Fe+Mg). Microphenocrysts and phenocryst rims are enriched in Fe relative to phenocryst cores (fig. 5).

Euhedral yellow fayalite phenocrysts up to 0.9 mm in diameter are rare but more common than garnet. They are compositionally homogeneous except for more Mg-poor, Mn-rich rims (fig. 5). They are similar in composition (table 6) to fayalitic olivines from high-silica

TABLE 7

Representative microprobe analyses of Fe–Ti oxides

	T-1	T-2	LC-1	T-1	LC-1
	magnetite			ilmenite	
SiO_2	0.17	0.15	0.12	0.11	0.11
Al_2O_3	2.51	2.83	0.75	0.21	0.00
FeO*	83.0	80.7	84.5	53.3	38.5
MgO	0.79	0.18	0.15	1.01	0.40
MnO	0.54	0.63	3.75	0.76	11.4
TiO_2	7.74	10.4	4.56	41.1	47.2
V_2O_3	0.20	0.02	0.10	0.09	0.02
ZnO	0.16	0.20	0.36	0.06	0.20
total	95.11	95.11	94.29	96.64	97.83
Fe_2O_3**	51.05	45.02	59.14	20.93	9.29
FeO**	37.06	40.19	31.29	34.47	30.14
total	100.22	99.62	100.22	98.74	98.76
	Formulae on the basis of 32 oxygens			... 6 oxygens	
Si	0.051	0.045	0.037	0.006	0.006
Al	0.884	1.004	0.269	0.013	0.000
Fe^{3+}	11.486	10.195	13.546	0.807	0.358
Fe^{2+}	9.267	10.113	7.965	1.476	1.289
Mg	0.352	0.081	0.068	0.077	0.030
Mn	0.137	0.161	0.969	0.033	0.494
Ti	1.740	2.353	1.044	1.583	1.815
V	0.048	0.005	0.024	0.004	0.001
Zn	0.035	0.044	0.031	0.002	0.008

* Total Fe as FeO.

** Recalculated from analysis.

rhyolites of Mono Craters (Carmichael, 1967) and the Coso Range (Bacon and Duffield, 1976 and unpub. data). The fayalite phenocrysts contain inclusions of apatite (table 9), zircon (table 10), rare pyrrhotite (table 8), and colorless glass. Zircon and apatite similar in composition to inclusions within fayalite and other phenocryst phases and to discrete microphenocrysts in the groundmass have been observed partially included within or adhering to the faces of fayalite phenocrysts (tables 9 and 10). Deep embayments filled with colorless glass connecting the adjoining groundmass with apatite inclusions are also found (pl. 1-A). Fayalite microphenocrysts are far more abundant and contain less Mg than phenocrysts (fig. 5). Some of these are as large as 0.2 mm but are distinguished from smaller phenocrysts by being hopper shaped. This texture is interpreted to indicate that microphenocrysts grew at cooling rates greater than might be expected in a static magma reservoir (Donaldson, 1976).

Garnet phenocrysts are generally euhedral, though some are slightly rounded, are deep red in hand specimen, about 0.5 to 1 mm in diameter, and account for 0.001 to 0.01 volume percent of the rock. Many garnet crystals have well-developed (110) faces with striations parallel to their edges (pl. 1-B). These are presumably due to growth-related phenomena. Except for thin rims enriched in Mn, probably due to growth during ascent, they are homogeneous almandines (table 6 and fig. 5).

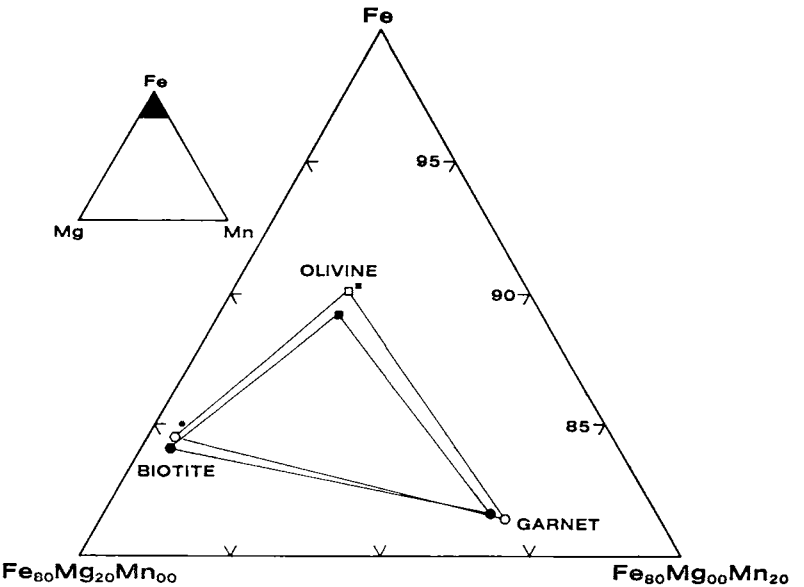

Fig. 5. Mafic silicate compositions of sample M-3, rhyolite of Monache Mountain, plotted in terms of atomic Fe–Mg–Mn (table 6). Tie lines connect coexisting cores (large filled symbols) and rims (large open symbols). Small filled symbols are microphenocrysts. Bi: biotite (hexagons); Fa: fayalite (squares); Gt: garnet (circles).

Garnet-bearing silicic volcanic and plutonic rocks have been described from a number of localities worldwide. In some occurrences garnet is evidently xenocrystic (Zeck, 1970), but in others, extremely high Mn content suggests the involvement of an aqueous vapor phase in a magmatic environment (for example, Leake, 1967). However, garnet is believed to be a primary magmatic phase in examples from a large number of occurrences (for example, Oliver, 1956; Green and Ringwood, 1968; Brousse, Bizourard, and Salat, 1972; Fitton, 1972; Birch and Gleadow, 1974; Wood, 1974; Kano and Yashima, 1976; Vennum and Meyer, 1979).

Perhaps the most persuasive evidence for the magmatic (that is, phenocrystic, rather than xenocrystic) origin of the garnets of Monache Mountain comes from their inclusions. In the cores of several garnet crystals are small inclusions of pyrrhotite rather similar in composition to pyrrhotite inclusions in fayalite phenocrysts (pl. 2-A and table 8). In

TABLE 8

Microprobe analyses of pyrrhotite inclusions in garnet and fayalite phenocrysts from rhyolite of Monache Mountain (M-3)

	Garnet	Fayalite
Cu	0.13	0.27
Ni	0.00	0.00
Co	0.00	0.00
Fe	61.9	61.8
Mn	0.17	0.10
S	38.9	38.5
Total	101.10	100.67

TABLE 9

Partial microprobe analyses of apatites from rhyolite of Monache Mountain (M-3)

	Fa core	Gt core	Gt	Bi	Fa/ GM	Gt/ GM	GM	GM	LG	LG
SiO_2	0.4	0.6	0.4	0.8	0.3	0.4	0.4	1.4	0.0	0.1
P_2O_5	41.0	41.2	40.9	41.0	42.1	40.9	41.4	41.2	41.5	41.2
CaO	53.2	53.1	53.0	53.0	53.5	53.3	53.7	52.7	53.2	53.6
FeO	2.7	1.9	1.8	1.1	2.0	1.7	1.3	1.1	0.5	0.9
Y_2O_3	0.12	0.15	0.14	0.14	0.10	0.12	0.16	0.13	0.04	0.00
La_2O_3	0.25	0.27	0.23	0.24	0.23	0.22	0.21	0.27	0.02	0.05
Ce_2O_3	0.59	0.64	0.61	0.66	0.58	0.61	0.57	0.74	0.18	0.19
Total	98.26	97.86	97.08	96.94	98.81	97.25	97.74	97.54	95.44	96.04

Fa: fayalite; Gt: garnet; Bi: biotite; GM: groundmass; LG: large grain; Fa/GM and Gt/GM: apatite partially included in phenocrysts.

TABLE 10

Partial microprobe analyses of zircons from rhyolite of Monache Mountain (M-3)

	Fa	Fa	Fa	Gt core	Gt	Gt	Gt/GM	GM	GM rim
Y_2O_3	0.71	0.59	0.47	0.60	0.33	0.18	0.37	0.84	0.18
HfO_2	1.26	0.85	1.00	1.05	0.69	0.83	1.14	1.25	0.93

Symbols same as table 9.

PLATE 1

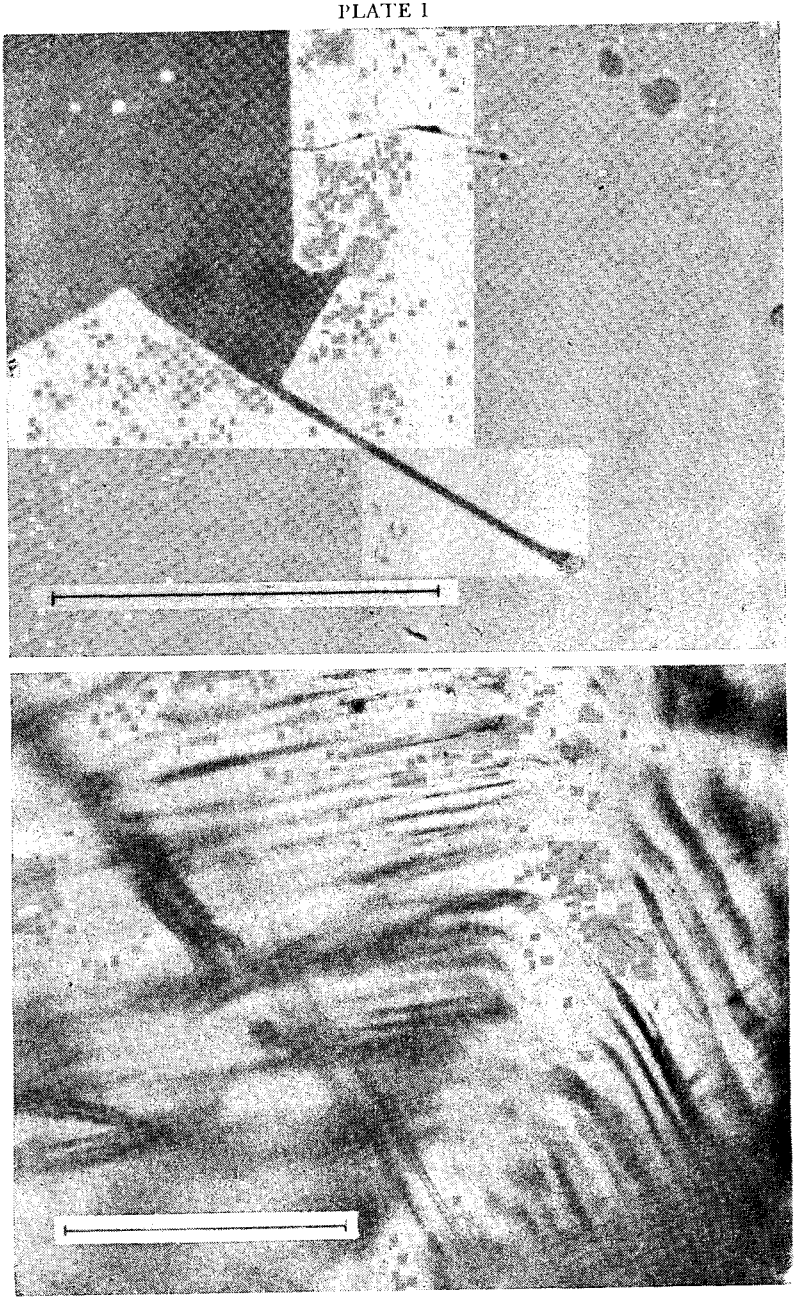

A.

B.

A. Margin of fayalite phenocryst (light gray) against groundmass (dark gray) showing apatite inclusions with long axes perpendicular to plane of photomicrograph (plane reflected light). Two of the apatite inclusions are connected with groundmass by sheets of glass. Bar in all plates is 0.1 mm long.

B. Garnet phenocryst in polished grain mount showing striations on crystal faces as seen through crystal (plane light). Several needles of apatite are visible as inclusions. Presence of striations suggests that garnet crystal was growing in melt.

PLATE 2

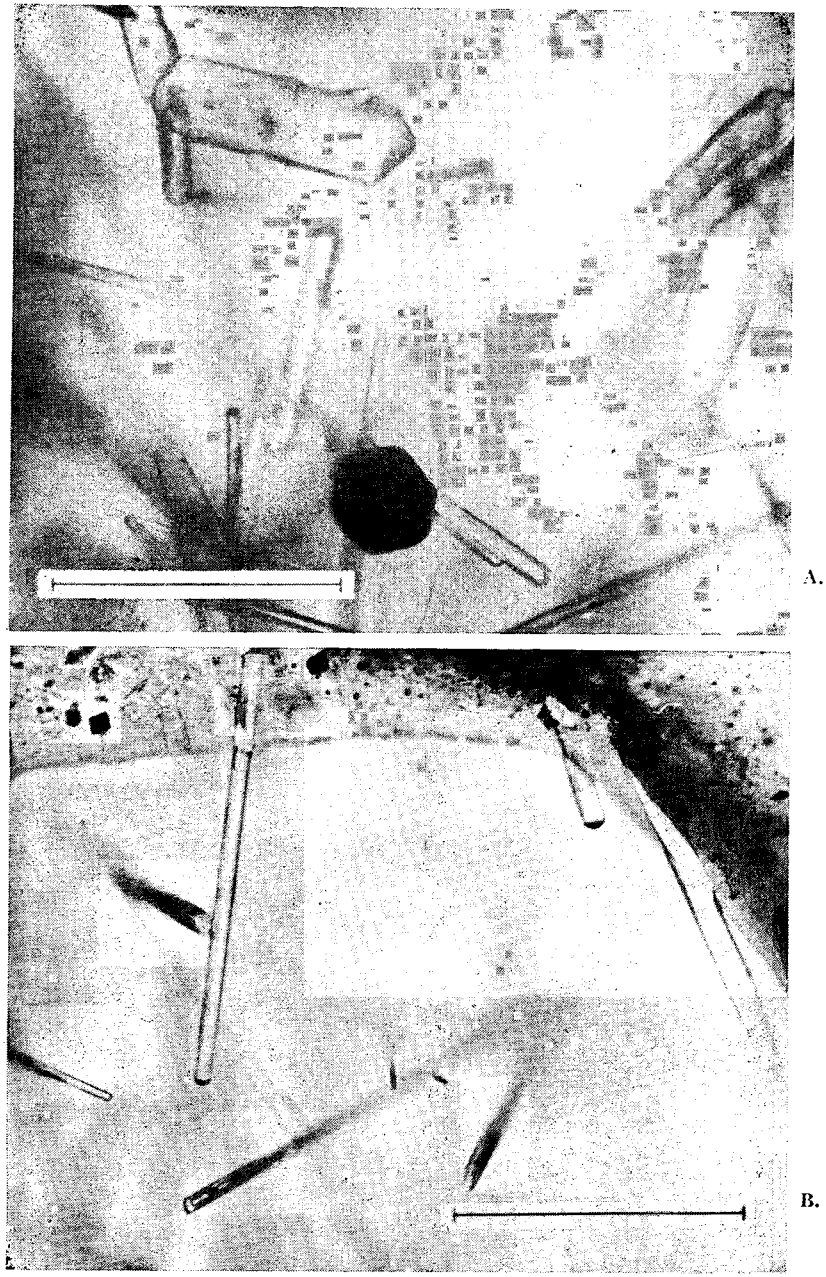

A.

B.

A. Inclusions in garnet phenocryst (plane light). Long needles are apatite, stubby prism in upper left is zircon, opaque is pyrrhotite. Hexagonal form of pyrrhotite probably reflects structure of host garnet.

B. Garnet phenocryst in polished grain mount showing apatite needles included in garnet and protruding into groundmass (plane light). Apatite in lower center contains glass inclusion with vapor bubble (black). Dark squares in groundmass are magnetite.

PLATE 3

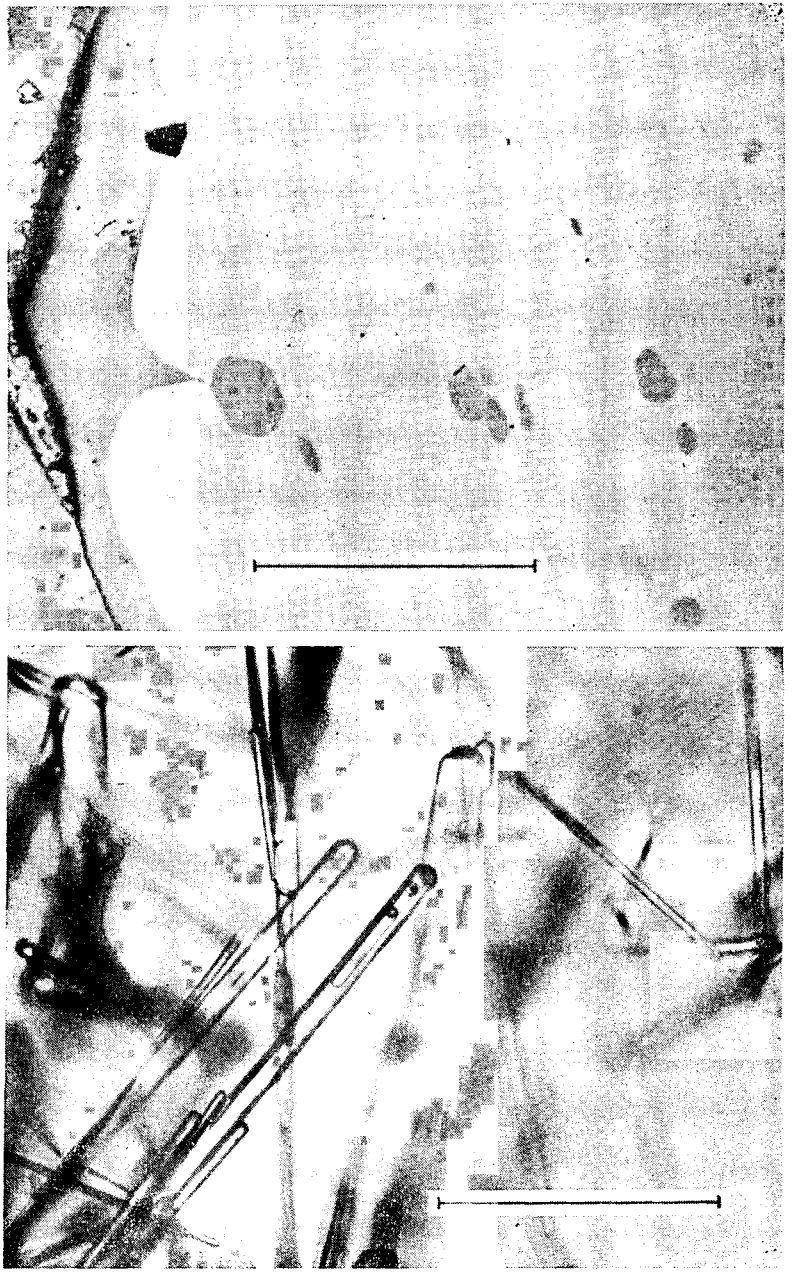

A.

B.

A. Margin of garnet phenocryst (light gray) against groundmass (dark gray) showing stages in process of inclusion of apatite (plane reflected light). Several apatite crystals are visible, with long axes perpendicular to plane of photomicrograph. Garnet crystal grew from right to left. Black portion of apatite at margin of garnet (upper left) is void caused by plucking during polishing.

B. Apatite inclusions in garnet phenocryst in polished grain mount (plane light). Apatite needle in center of field contains inclusion of glass with small vapor bubble.

addition, garnet crystals include abundant needles of apatite, some of which protrude at least 0.05 mm into the surrounding glassy groundmass (pl. 2-B). Various stages in the process of inclusion of apatite can be seen in a single garnet crystal (pl. 3-A). Apatite inclusions appear to be more numerous in the cores of garnet crystals, but no regions are entirely free of apatite needles. A few apatites have inclusions of colorless glass in their cores, greatly elongated parallel to the long axis of the crystals and showing one or more vapor bubbles (pls. 2-B and 3-B). Observation of the bubbles with a microscope equipped with a freezing stage revealed no condensable material, solid or liquid, within the bubbles, suggesting they are due to differential contraction during cooling.

The Y, La, and Ce contents of the apatites are within the range of composition of discrete microphenocrysts in the groundmass and inclusions in fayalite and biotite phenocrysts (table 9). Very rare large apatite crystals that may be xenocrystic are quite different in composition from apatite inclusions and microphenocrysts (table 9). Though less abundant than apatite, zircon inclusions in garnet are compositionally similar to microphenocrysts of zircon in the groundmass and inclusions in fayalite phenocrysts (table 10).

Rhyolite of Long Canyon

The rhyolite of Long Canyon (sample LC-1) is distinctly porphyritic, containing about 20 percent euhedral quartz, plagioclase, and sanidine phenocrysts between about 0.2 and 1 mm in size (table 5). These phases commonly occur intergrown in clots up to 4 mm in diameter. Sanidine and most plagioclase phenocrysts are unzoned except for thin, relatively sodic rims. Rare euhedral plagioclase crystals have somewhat more calcic cores and show faint oscillatory zonation (fig. 4). Rare inclusions of biotite and Fe–Ti oxides are present in all the salic phases.

Brown biotite forms subhedral to euhedral microphenocrysts and phenocrysts up to 0.8 mm in diameter. Biotite phenocrysts are very rich in Mn (table 6) and unzoned except for a slight decrease in Ti content toward the margins. They contain much more F than biotite phenocrysts from Monache and Templeton Mountains. Biotite inclusions in feldspars and quartz contain as much as 1.6 percent F. Many biotite crystals occur in clots with magnetite and/or ilmenite. Sparse inclusions of Fe–Ti oxides and abundant needles of apatite are present in some of the larger biotite phenocrysts.

Microphenocrysts of magnetite and ilmenite are euhedral and up to 0.2 mm in longest dimension. They are homogeneous, poor in Al, and unusually rich in Mn (table 7) compared to fresh Fe–Ti oxides from many other silicic volcanic rocks (Carmichael, 1967; Lipman, 1971; Evans and Nash, 1975; Bacon and Duffield, 1976; Hildreth, 1979). Minute inclusions of apatite and glass are present in some examples of both phases.

The groundmass of LC-1 is composed of colorless glass laced with microlites that are oriented preferentially and concentrated in layers that define flow banding. Glassy areas show perlitic cracks around ~1

mm diameter nonhydrated cores that are poorer in Ca and richer in K than the whole rock (table 2). The F content of the glass is rather high at 0.6 percent. The normative feldspar composition of the glass is appropriate for a quartz-saturated liquid in equilibrium with plagioclase and sanidine (fig. 4).

PETROGENESIS

The presence of the rhyolites of Templeton and Monache Mountains and Long Canyon atop the Kern Plateau is probably linked to the existence of late Cenozoic mafic volcanic rocks nearby (fig. 2). By analogy with other "bimodal" volcanic fields in the Western United States, it is assumed that the rhyolites of the Kern Plateau are products of partial melting of crustal rocks, brought about principally by intrusion of mafic magma from the mantle (Lachenbruch, 1978/79). To what extent the silicic melts have been modified during their ascent from the sites of partial fusion is difficult to assess, especially in a field with but four known occurrences. Nonetheless, certain inferences can be drawn concerning the nature of the magmatic systems that fed these domes and the physical conditions that most likely prevailed within them.

Templeton Domes

Because Templeton Mountain and Little Templeton Mountain are partly overlapping domes of similar age, they should be considered together in a discussion of petrogenesis. Many features that suggest a close genetic relation were described earlier. Most of these would appear to be capable of explanation by a model emphasizing crystal-liquid equilibria. Three cases are considered:

Case 1: separation of phenocrysts.—A glance at the analytical data invites one to derive a liquid of T-2 composition from one of T-1 composition by separation of phenocrysts found in the latter. A least-squares analysis of this problem was performed for major elements and Zr using a modified version of the program of Wright and Doherty (1970), with each mass balance equation weighted in accordance with the inverse of its absolute error (Reid, Gancarz, and Albee, 1973). The analyses of phenocrysts from T-1 given in tables 6 and 7, plagioclase of composition $An_{38.3}Ab_{59.4}Or_{2.3}$, and ideal zircon and apatite were employed, with $Fe_2O_3/(FeO + Fe_2O_3)$ estimated for ferromagnesian silicates. Subtraction of 7 percent plagioclase, 1 percent hypersthene, 0.5 percent ilmenite, 0.06 percent apatite, and 0.02 percent zircon from sample T-1 produces a calculated liquid composition similar to the bulk analysis of T-2 but unacceptably high in SiO_2 and low in Al_2O_3, Fe_2O_3, MnO, Na_2O, and K_2O. The discrepancies in Na_2O and Fe_2O_3 may be due to post-magmatic effects. However, the other inconsistencies argue against separation of phenocrysts alone to produce T-2 from T-1.

Trace-element evidence qualitatively favors the phenocryst separation model with the important exception of Ba. Partition coefficients for a number of crystalline phases relative to silicic melts (Arth, 1976; Hildreth, ms) show that the only observed phenocryst phase capable of strongly fractionacting Ba ($D >> 1$) needed to deplete its concentration

in T-2 by nearly a factor of 2 is biotite. However, separation of biotite would deplete the liquid in K, Rb, Cs, Mn, and Zn, elements that are enriched in T-2. Even if sanidine were present, its separation would also fail to satisfy the Ba depletion requirement because of the obvious sympathetic decrease in K. In addition, the opposite sense of enrichment of Co and Zn is difficult to reconcile with crystal fractionation alone.

Separation of phenocrysts suffers as a model on geologic as well as geochemical grounds. Hornblende is an abundant, early-formed phase in T-1 (table 5) that is a prime candidate for separation, yet the least-squares calculation favors an assemblage lacking amphibole phenocrysts. In addition, were T-2 to be derived from T-1 by complete separation of some assemblage of crystalline phases, crystallization would have to be interrupted and then proceed again to a greater extent prior to eruption. Thus, it seems likely that the difference in bulk composition existed before precipitation of the observed phenocrysts.

Case II: incremental melting.—An alternative hypothesis to separation of phenocrysts has liquid of T-2 composition extracted from a zone of partial melting, followed by extraction of liquid of T-1 composition. Once segregated from residual crystals, the magmas must have been held either in separate reservoirs or in a single compositionally zoned reservoir while phenocrysts grew under apparent equilibrium conditions.

Helz (1976) showed that peraluminous, rhyolitic glasses can be produced by approx 10 percent partial melting of tholeiitic basalt under H_2O-saturated conditions at 700°C and 5 kb, under which conditions hornblende is a major residual phase. With increasing temperature, melts become less silicic, but Fe/(Fe + Mg) remains high, until appreciable hornblende enters the melt at above 900° to 1000°C. Effects of varying oxygen fugacity on melt composition are small throughout the temperature range of stability of hornblende. Presumably, so long as the fugacity of H_2O is sufficient to stabilize hornblende, similar results would be obtained at higher total pressures and H_2O undersaturation.

The silicic, MgO-poor character of partial melts in equilibrium with hornblende would be expected to persist to higher temperatures in systems of intermediate bulk composition. Some peraluminous rhyolites might thus be derived by partial melting of metaigneous, rather than pelitic metasedimentary, source rocks. The $^{87}Sr/^{86}Sr$ value of 0.7064 for T-1 could more easily be reconciled with such an origin. REE partition coefficients for hornblendes in dacitic and more silicic rocks are generally much greater than unity and far higher for heavy than light REE (Arth, 1976). Thus, the high La/Sm and La/Yb of the Templeton Mountain rhyolites are also qualitatively consistent with residual hornblende as a major control on composition.

The differences in major-element content between T-2 and T-1 are similar in trend to those observed by Helz (1976) for increasing temperature and, consequently, melt fraction. The presence of hornblende phenocrysts in the less silicic melt would then be due to a greater contribution of hornblende components from the source. Partial melting

calculations (Shaw, 1970) and inspection of partition coefficients for phenocrysts from silicic volcanic rocks (Arth, 1976; Hildreth, ms) indicate that differences in Ba, Rb, Ce, Eu, and Yb between T-1 and T-2 can probably be accounted for by varying degrees of partial melting of intermediate rocks. K-feldspar, plagioclase, biotite, hornblende, and magnetite would be residual phases in the melting event that produced T-2. Further melting, such that K-feldspar would be entirely consumed, would produce a liquid enriched in Ba and depleted in K in the manner of composition T-1. Complexities of trace-element behavior (Albarede and Bottinga, 1972) and lack of independent constraints on source mineralogy and modal composition preclude more rigorous evaluation of partial melting models.

Case III: liquid-state fractionation.—Some of the compositional differences between T-1 and T-2 might be explained by a process involving the fractionation of elements in a compositionally zoned magma reservoir without the removal or addition of crystals (Shaw, Smith, and Hildreth, 1976). Such a process is apparently related to upward migration of H_2O and halogens and has been shown to have operated in the magma chamber of the Bishop Tuff (Hildreth, 1979). The greater enrichment of heavy REE in T-2 relative to light REE, enrichment in Mn, Fe, Zn, Rb, Cs, Ta, Th, and U, and depletion of Mg, Ba, and Eu in T-2 might be explained in this way. However, many chemical features cannot (for example, K-content), and, if the two magmas are consanguineous, some appeal must be made to crystal/liquid fractionation processes.

The simplest model that satisfies all constraints imposed by the chemical and mineralogical data combines the petrogenetic processes of cases II and III. In this scenario, crystal-free melt of composition T-2 separated from residual crystals and migrated to some holding reservoir. This migration was followed by further partial fusion and separation of melt of composition T-1, which may have lodged beneath T-2. Mild liquid-state fractionation and precipitation of phenocrysts, without significant settling, proceeded within the reservoir. The relative absence of zonation in the plagioclase of T-2, in contrast to zonation in plagioclase of T-1, may reflect higher activity of H_2O in T-2, as implied by case III. Higher activity of H_2O would lower viscosity and presumably increase diffusion rates in the melt, inhibiting the development of oscillatory zoning in plagioclase (Sibley and others, 1976). Microphenocrysts probably formed during ascent and early cooling of the magma.

Phenocryst equilibration.—An estimate of the temperature and fugacity of oxygen during equilibration of the phenocrysts in T-1 that is virtually independent of pressure can be obtained from the compositions of coexisting magnetite and ilmenite (table 7). The assumption that the phenocryst compositions record a state of chemical equilibrium in a magma reservoir is considered valid since Fe–Ti oxides and ferromagnesian silicates are virtually unzoned, and oxide crystals included within hypersthene and hornblende are compositionally very similar to large, discrete oxide phenocrysts. Recalculation of the oxide analyses

and estimation of their equilibration temperature by the method of Carmichael (1967), using the data of Buddington and Lindsley (1964), yields 860°C at an oxygen fugacity of $10^{-11.6}$ bars. Recent experimental work by Lindsley and coworkers has added significantly to the data presented by Buddington and Lindsley (1964). Normalization of analyses to account for the effects of Mn, as suggested by Lindsley (written commun., 1976), and use of his solution model (written commun., 1977) which incorporates all the experimental data, give a temperature of 910°C at an oxygen fugacity of $10^{-10.4}$ bars. The latter estimate is plotted in figure 6, along with estimates by the same method for phenocrysts in the compositionally and mineralogically similar dacites of the Lassen Peak area (Carmichael, 1967, nos. 28 and 29).

Experimental studies of H_2O-undersaturated granitic melts suggest that the temperature obtained for T-1 (910°C) is near the upper limit

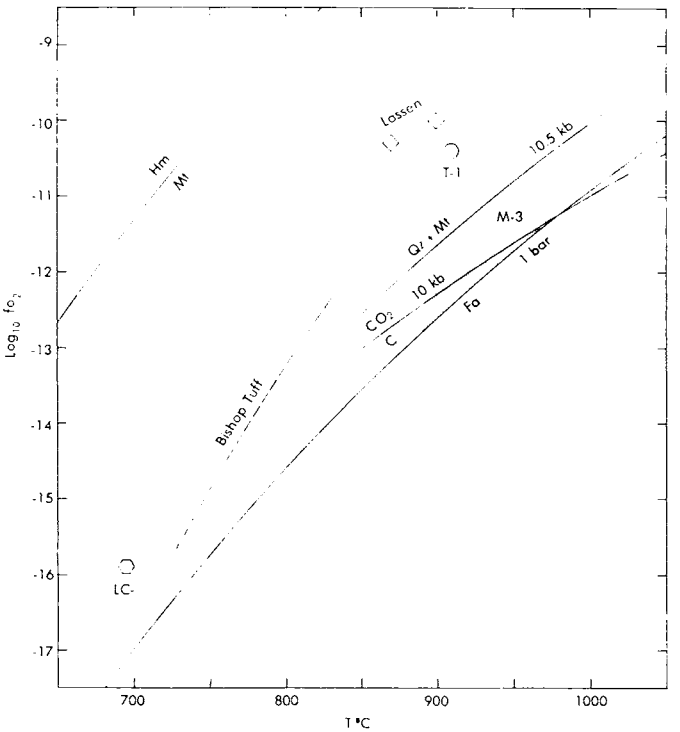

Fig. 6. Oxygen fugacity versus temperature. Plotted points and curve for Bishop Tuff (Hildreth, ms) are based on compositions of coexisting Fe–Ti oxides calculated by the methods of Lindsley (see text); hexagon: rhyolite of Long Canyon (LC-1, table 7); circle: rhyolite of Templeton Mountain (T-1, table 7); diamonds: Lassen dacites (Carmichael, 1967, nos. 28 and 29). Upper part of shaded area applies to phenocrysts in rhyolite of Monache Mountain (M-3), lower part to groundmass. Curve labeled 1 bar is fayalite (Fa)–magnetite (Mt)–quartz (Qz) buffer determined by Hewitt (1978); 10.5 kb is Hewitt's (1978) buffer corrected to that pressure, as described in text; graphite (C)–CO_2 curve is based on the data of Robie, Hemingway, and Fisher (1978) corrected to 10 kb using the fugacity coefficients of Shmulovich and Shmonov (1975); hematite (Hm)–magnetite (Mt) curve is from Eugster and Wones (1962).

of stability of biotite and hornblende (Naney, ms; Wyllie, 1977). Phase equilibrium data are unavailable for bulk compositions sufficiently like that of the rhyolite of Templeton Mountain to provide a rigorous evaluation of hydrous ferromagnesian silicate stability. Assuming that the phenocrysts represent near-liquidus phases, the estimated equilibration temperature and the phase equilibrium data reviewed by Wyllie (1977) imply that the Templeton magma contained less than about 4 wt percent H_2O.

Source rocks.—Determination of the source rock for the Templeton Mountain rhyolites is complicated by effects of fractionation processes. Rb, Sr, and $^{87}Sr/^{86}Sr$ in T-1 argue against derivation by partial melting of metasedimentary or ancient crustal rocks. To the extent that the rhyolites represent melts unmodified by events beyond partial fusion, their chemical compositions appear to be consistent with initial derivation by small to moderate degrees of partial melting of plutonic or metavolcanic rocks of intermediate composition. The presence of hornblende phenocrysts in T-1 and its major-element composition are consistent with such a source, as suggested for "I-type" granites by White and Chappell (1977).

Monache Mountain

A major question to be addressed regarding the rhyolite of Monache Mountain is whether its unusual chemical composition reflects the source rocks, processes acting in a deep magma reservoir, or fractionation during ascent. The last of these can be eliminated because of mineralogic evidence for rapid ascent and survival of a high-pressure phenocryst assemblage.

Equilibration of phenocrysts.—Several lines of evidence indicate that garnet, fayalite, biotite, and plagioclase phenocrysts preserve a record of equilibrium conditions in a magma reservoir. The absence of significant compositional zonation for all but rims of crystals, the presence of similar suites of inclusions, and generally euhedral habit argue for relatively slow, equilibrium crystallization. Hopper-shaped fayalite microphenocrysts suggest rapid growth during ascent and cooling, events that took place in a shorter period of time than for striations on garnet faces, apparently due to growth-related phenomena, to be completely removed by dissolution. Furthermore, the phenocryst assemblage and the compositions of the phases are consistent with equilibration under conditions appropriate for the formation of rhyolite magma in the lower crust.

A reasonable approximation to the temperature and pressure of equilibration can be obtained from the phenocryst compositions and experimental and thermodynamic data for the reactions

$$\underset{\text{almandine}}{Fe_3Al_2Si_3O_{12}} + \underset{\text{phlogopite}}{KMg_3AlSi_3O_{10}(OH)_2} = \underset{\text{annite}}{KFe_3AlSi_3O_{10}(OH)_2} + \underset{\text{pyrope}}{Mg_3Al_2Si_3O_{12}} \quad (1)$$

$$\underset{\text{anorthite}}{3CaAl_2Si_2O_8} + \underset{\text{fayalite}}{3Fe_2SiO_4} = \underset{\text{grossular}}{Ca_3Al_2Si_3O_{12}} + \underset{\text{almandine}}{2Fe_3Al_2Si_3O_{12}} \quad (2)$$

Ferry and Spear (1978) investigated (1) at 2.07 kb and 550° to 800°C and presented an equation (Ferry and Spear, 1978, eq 7) for the pressure and temperature dependence of (Mg/Fe) garnet/(Mg/Fe) biotite based on their experimental results and the volume change for the reaction at 298K. They suggested that this equation is applicable to compositions of garnet and biotite for which $0.80 \leqslant Fe/(Fe+Mg) \leqslant 1.00$ and that it is a useful geothermometer for natural biotite of $(Al^{VI}+Ti)/(Al^{VI}+Ti+Fe+Mg)$ up to about 0.15 and garnet of (Ca+Mn)/(Ca+Mn+Fe+Mg) up to about 0.2. These conditions are very nearly satisfied by the garnet and biotite phenocrysts from the rhyolite of Monache Mountain. The resulting, nearly pressure-independent curve is shown in figure 7.

Reaction (2) was studied experimentally by Green and Hibberson (1970) and was applied to natural systems by Wood (1975, eq 15). Using the composition of phenocrysts in M-3, the curve shown in figure 7 is obtained. It is only mildly temperature dependent, intersecting the curve for (1) at a high angle. These data imply that the phenocrysts in M-3 equilibrated at 980 ± 50°C and 10.5 ± 3.0 kb, the uncertainties being taken from Ferry and Spear (1978) and Wood (1975). Calculation of equilibration temperature necessitates extrapolation of the ln K versus 1/T relationship obtained by Ferry and Spear (1978, fig. 3) to higher temperatures and pressures. Phase equilibrium studies of granitic melts suggest that 980 ± 50°C may exceed the stability of biotite by approx

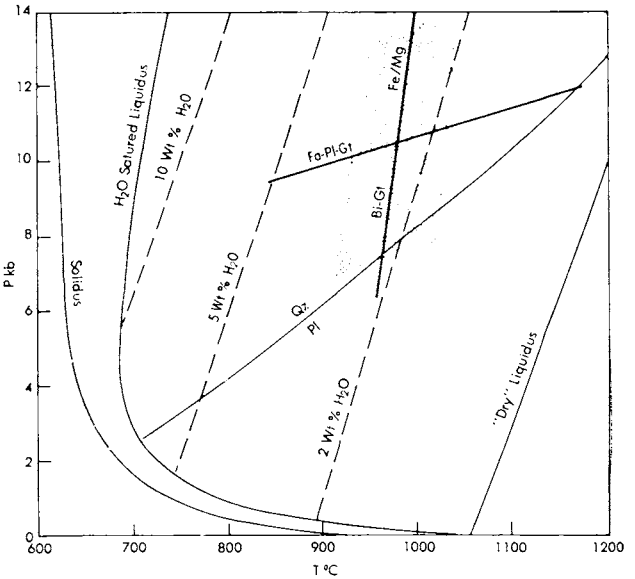

Fig. 7. Pressure versus temperature diagram showing calculated equilibria for phenocrysts in rhyolites of Monache Mountain (M-3) (heavy curves), with area of overlap in uncertainties for both curves indicated by shading. Fa–Pl–Gt curve based on eq 15 of Wood (1975); Bi–Gt based on eq 7 of Ferry and Spear (1978); other curves after Wyllie (1977, fig. 6). Dashed lines are liquidi for indicated H_2O contents; Qz/Pl curve separates areas of the primary crystallization of quartz and plagioclase.

100° (Naney, ms; Wyllie, 1977), but compositions as Al- and Fe-rich as the Monache rhyolite have apparently not been investigated. The small amount of F in the biotite (table 6) alone is probably insufficient to account for this discrepancy. If the phenocryst assemblage does indeed record a state of chemical equilibrium the temperature may have been close to the lower limit of the stated uncertainty.

Also shown in figure 7 are experimentally determined liquidus curves for varying H_2O content for granitic magma (Wyllie, 1977, fig. 6). Since the rhyolite of Monache Mountain contains few phenocrysts and may have been at near-liquidus temperature when the phenocrysts equilibrated, the experimental data suggest that the magma contained less than 4 wt percent H_2O at this point in its history. The fact that the calculated equilibration curves intersect in the primary phase field of quartz (fig. 7), rather than plagioclase, is probably due to the more Q-rich normative composition of the material studied experimentally (Wyllie, 1977, table I, no. 104).

The pressure, temperature, and H_2O content obtained for the Monache rhyolite magma are similar to those deduced by different methods by Wood (1974) for garnet crystallization in rhyolites from Canterbury, New Zealand. The equilibration temperature and H_2O content estimated for the Monache magma are in the same range as those indicated for the rhyolite of Templeton Mountain.

Attempts to synthesize garnet from molten silicic volcanic rocks (Green and Ringwood, 1972) and to produce silicic melts from pelitic rocks containing garnet (Green, 1976) have not succeeded in producing the almandine-rich compositions of phenocrysts found in volcanic rocks. Part of this discrepancy may be due to higher bulk Mg/Fe of the experimental systems, as noted by Wood (1974). Part may be due also to oxygen fugacity, which was not controlled in the experiments and may have been much higher than in natural systems.

The fugacity of oxygen was evidently relatively low, compared to most high-temperature silicic volcanic rocks, when the phenocryst assemblage in the rhyolite equilibrated. This conclusion may be inferred from the silicic nature of the magma, the presence of nearly pure fayalite, and the absence of magnetite. Though quartz has not been found as a phenocryst in M-3, the activity of SiO_2 relative to β-quartz was probably near unity (fig. 7). Therefore, the fugacity of oxygen was below that defined by (3) at the appropriate temperature and pressure:

$$\underset{\beta\text{-quartz}}{3SiO_2} + \underset{\text{magnetite}}{2Fe_3O_4} = \underset{\text{fayalite}}{3Fe_2SiO_4} + \underset{\text{gas}}{O_2} \qquad (3)$$

The equilibrium curve for (3) is shown as a function of temperature and $\log_{10}f_{O_2}$ in figure 6, corrected to a pressure of 10.5 kb using appropriate molar volumes, coefficients of thermal expansion, and compressibilities for the solid phases. Thus, the phenocrysts in M-3 equilibrated at oxygen fugacities perhaps two orders of magnitude below those in other biotite-bearing, high-temperature rhyolites where temperature and oxygen fugac-

ity are obtained from the compositions of coexisting Fe–Ti oxides (Carmichael, 1967). Such relatively low oxygen fugacity is consistent with the stability of almandine (Hsu, 1968; Keesman and others, 1971). Similar conclusions were reached by Wood (1974) for almandine-bearing rhyolites that contain ubiquitous early-crystallizing ilmenite with very low Fe^{3+} as the sole Fe–Ti oxide phase. Oxygen fugacity in the Monache magma was appropriate for the co-precipitation of fayalite and nearly Ti-free magnetite at the time of groundmass crystallization.

The relatively low oxygen fugacity indicated by the phenocryst assemblage may be due to (4) if graphite were present in the source rocks (Ishihara, 1977).

$$\underset{\text{graphite}}{C} + \underset{\text{gas}}{O_2} = \underset{\text{fluid}}{CO_2} \qquad (4)$$

Since the Monache Mountain magma was apparently undersaturated in H_2O and since the solubility of CO_2 in silicate melts at high pressure is much less than that of H_2O, a fluid phase would be rich in CO_2 (Holloway, 1976). The fugacity of O_2 defined by (4) for pure graphite and CO_2 fluid has been calculated at 10 kb from the fugacity coefficients of Shmulovich and Shmonov (1975) and the Gibbs Free Energy of formation data of Robie, Hemingway, and Fisher (1978). The resulting curve is plotted in figure 6. The oxygen fugacity so defined is appropriate for the stability of fayalite and absence of magnetite phenocrysts in the rhyolite, though evidence for the presence of graphite in the source rocks is lacking.

Possible source rocks.—The phenocryst equilibration conditions, textural features, and inclusion suites indicate that phenocrysts grew in a melt at roughly 30 km depth. Since there is no evidence for existence of earlier formed phenocrysts or liquid-state fractionation of the type described by Shaw, Smith, and Hildreth (1976), the bulk composition of M-3 must reflect partial melting of lower crustal rocks. The high La/Yb, Fe/(Fe+Mg), and peraluminous character imply that hornblende and/or garnet could have been residual phases. The negative Eu anomaly, high Rb/Sr, and low Sr indicate residual plagioclase and possibly K-feldspar. The high K content and Ba abundance similar to T-2 imply that K-feldspar and/or biotite may have been residual phases. The extremely high Fe/(Fe+Mg) requires either a small degree of partial melting or an extremely Fe-rich source. The $^{87}Sr/^{86}Sr$ ratio of 0.7059 and $\delta^{18}O$ of 7.8 preclude a deep crustal metasedimentary source, though the Ca-poor, Fe-rich composition and inferred low oxygen fugacity may be more readily explained if appeal be made to a source that has been affected by weathering processes, as for many "S-type" granites (White and Chappell, 1977). The implications of the isotopic data may be reconciled with the chemical composition (for example, Fe/(Fe+Mg), Rb/Sr), if the rhyolite of Monache Mountain represents a comparatively small degree of partial melting of deep crustal rocks of igneous parentage.

Many of the differences between the Templeton and Monache Mountain rhyolites may be due to differences in source rocks that are reflected in the surface exposures of basement rocks and in the regional gravita-

tional field. The Templeton domes lie at the margin of the large compositionally zoned granodiorite of the Late Cretaceous Whitney pluton (Moore and du Bray, 1978), whereas in the vicinity of Monache Mountain are extensive exposures of older metamorphic and more mafic igneous rocks (Matthews and Burnett, 1965). A large area south of Monache Mountain is characterized by Bouguer gravity values about 20 mgal in excess of those implied by the regional gradient (Oliver and Robbins, 1979). The location of Monache Mountain within the zone of decreasing Bouguer gravity between this high and the Whitney pluton to the north implies that differences in basement composition at the surface may persist to great depth. More mafic source rocks for the rhyolite of Monache Mountain than for those of Templeton Mountain would be consistent with its lower $^{87}Sr/^{86}Sr$. If the similar calculated phenocryst equilibration temperatures reflect melting conditions, then the apparently lower degree of partial melting implied by the composition of the Monache rhyolite is also consistent with a more mafic source.

Long Canyon Dome

Chemical analyses of the rhyolite of Long Canyon suggest that its petrogenesis was dominated by the same processes that governed the development of many other late Cenozoic high-silica rhyolites from the Western United States. Homogeneous populations of crystals, feldspar-glass relations (fig. 4), and the absence of significant compositional zonation of phenocrysts indicate that chemical equilibrium prevailed at least locally in the magma reservoir prior to eruption.

Equilibration of phenocrysts.—Temperature and oxygen fugacity at the time of equilibration have been estimated from the compositions of the coexisting Fe–Ti oxides. These values are subject to considerable uncertainty owing to the high Mn content of the oxides (table 7). Recalculation of the analyses by the methods of Carmichael (1967) and Lindsley (written commun., 1976) yield identical results for ulvospinel and ilmenite mole fractions. Comparison with the experimental data of Buddington and Lindsley (1964) gives an equilibration temperature of 640°C at an oxygen fugacity of $10^{-18.1}$ bars; use of Lindsley's solution model based on more extensive experimental data gives 695°C at an oxygen fugacity of $10^{-15.9}$ bars. The higher temperature is probably the more accurate because it more nearly approximates an appropriate position within the experimentally determined melting interval of H_2O-rich granitic compositions at low to moderate pressure (Wyllie, 1977).

The highly sodic composition of plagioclase and potassic sanidine in LC-1 suggests a relatively low equilibration temperature. The two-feldspar geothermometer of Stormer (1975) gives 606°C at 1 kb pressure. However, as Stormer (1975) pointed out, calculated values for systems with potassic plagioclase may be significantly in error owing to the binary albite–anorthite solution model employed by the geothermometer. It is unlikely that feldspar phenocrysts equilibrated at a temperature significantly different from the oxides. The temperatures calculated from

the oxide compositions are considered more representative of magmatic conditions.

The apparent phenocryst equilibration temperature of 695°C suggests that the magma was characterized by a high activity of water. The inception of biotite crystallization apparently before that of quartz and feldspars and the absence of other mafic silicates is suggestive of high H_2O content (Maaløe and Wyllie, 1975; Naney, ms). The pattern of enrichment in heavy REE relative to light REE with a large negative Eu anomaly (fig. 3) is distinctly like REE patterns for high-silica rhyolites that are thought to represent water-rich magma (for example, Hildreth, 1979). Similarly, high content of Sc, Mn, Rb, Sb, Cs, Ta, Th, and U and low Mg, P, Ti, Sr, and Ba may be related to high water activity. Unfortunately, water activity and content cannot be quantified with sufficient accuracy from the phenocryst compositions alone, especially since total pressure also cannot be tightly constrained.

Differentiation.—The rhyolite of Long Canyon is clearly a highly evolved rock. Its chemical composition has many of the characteristics of highly differentiated magmas erupted from crustal reservoirs (Smith, 1979). The processes acting to produce this extreme composition, probably including liquid-state fractionation (Shaw, Smith, and Hildreth, 1976; Hildreth, 1979), have largely obscured any record of the parental magma and source rocks.

Rare, small, relatively calcic cores of plagioclase phenocrysts are suggestive of involvement of higher temperature and, perhaps, less silicic magma at some point in the evolution of LC-1. These andesine cores are probably too sodic to be restite material. Perhaps they are xenocrysts from granitic wall rock, or possibly they may have been derived from a convecting, less silicic magma that may have underlain a stagnant, water-rich cap of high-silica rhyolite magma, now represented by LC-1, in the manner envisaged by Smith (1979) and Hildreth (1979).

DISCUSSION

The ages and petrogenetic histories of rhyolites from the Kern Plateau have significant implications for the late Cenozoic tectonic and thermal regimes of the southern Sierra Nevada. The Kern Plateau lies immediately west of the Basin and Range province (fig. 1) and seems to reflect the same regional stress field and pattern of late Cenozoic volcanic activity.

Approximately 40 km southeast of Long Canyon is the late Cenozoic Coso volcanic field (fig. 1; Babcock, 1975; Duffield, Bacon, and Dalrymple, 1980). Basaltic volcanism at Coso is interpreted as a consequence of extension of the lithosphere recorded by north-northeast-trending normal faults; mantle-derived basaltic magma was probably injected as dikes in response to such extension (Lachenbruch, 1978/79). Two volume maxima occur in basaltic volcanism in the Coso field (Duffield, Bacon, and Dalrymple, 1980): (1) between about 4 and 3 m.y., with a maximum at 3.6 m.y., the age of basalt that caps the Kern Canyon fault 20 km west-southwest of Monache Mountain (Dalrymple, 1963); and (2) between about 1.1 m.y.

and late Pleistocene time, probably bracketing the age of basalt 10 km west-northwest of Templeton Mountain (fig. 2).

Silicic magmas of the Coso volcanic field probably formed as partial melts of the crust as heat from intruded basalt sufficiently increased temperatures (Duffield, Bacon, and Dalrymple, 1980). A similar origin is proposed for the rhyolites of the Kern Plateau. Moreover, the greatest volume of silicic rocks at Coso consists of rhyodacite erupted between 3.1 and 2.5 m.y., with the first eruptive products being pyroclastic, the last lava flows and domes (Duffield, Bacon, and Dalrymple, 1980); small volumes of highly differentiated high-silica rhyolite were emplaced as domes and flows during the Pleistocene period of basaltic volcanism (Babcock and Wise, 1973; Bacon, Duffield, and Nakamura, 1980), with most of the rhyolite having been erupted since about 0.3 m.y. ago (Duffield, Bacon, and Dalrymple, 1980). At Coso, as on the Kern Plateau, the most voluminous, least SiO_2-enriched silicic magmas and the more highly evolved, most silicic magmas were erupted at roughly the same times.

Why was the intensity of volcanism so different in the two areas? The difference may be explained by the contrast in late Cenozoic deformational style between the Basin and Range and Sierra Nevada tectonic provinces. Both share the same general stress field, with maximum horizontal compression in a north-northeast sense in the region considered here. However, in the Basin and Range there is a significant component of lithospheric extension in addition to the northwest right-lateral and northeast left-lateral shearing evident in both provinces (Lockwood and Moore, 1979). That is, the axis of minimum compressive stress (σ_3) has been horizontal and oriented west-northwest in both regions, but the axis of maximum compressive stress (σ_1) has apparently been horizontal and oriented north-northeast in the Sierra Nevada, while nearby in the Basin and Range it (σ_1) has alternated between this orientation and a vertical one (Walter and Weaver, 1980).

It is proposed that in the Kern Plateau region a sufficient component of extension has allowed intrusion of basalt into the crust during at least part of late Cenozoic time. The result is a component of advective heat transfer by basaltic magma from asthenosphere to lithosphere, as suggested by the model of Crough and Thompson (1977, p. 399) for regional uplift and heat flow relations in the Sierra Nevada. More frequent and voluminous volcanism and higher heat flow occur east of the Sierra Nevada, where the rate of extension is much greater. When extension rates were apparently greatest, basalt or rhyolite was erupted, having reached the surface via dikes whose most probable azimuth was north-northeast (Bacon, Duffield, and Nakamura, 1980). Eruption of the rhyolite of Long Canyon coincident with a linear topographic depression of this trend that is parallel to many other major lineaments in the region and the similar orientation of a line defined by the two Templeton domes (fig. 2) may thus reflect the axis of maximum horizontal compressive stress (Nakamura, 1977). This is the direction of maximum horizontal

compressive stress defined by normal faults and seismicity east of the Sierra Nevada (Wright, 1976; Bacon, Duffield, and Nakamura, 1980; Walter and Weaver, 1980) and by apparently young microfaults in this part of the Sierra Nevada (Lockwood and Moore, 1979).

The apparently deep reservoirs for the high-temperature Pliocene rhyolites of the Kern Plateau may indicate that those magmatic systems were tapped at comparatively early stages in their evolution. It seems likely that the small volume of phenocryst-rich, low-temperature rhyolite of Pleistocene age would have been erupted from a much shallower reservoir. The apparent protracted differentiation and probable shallow reservoir for the Pleistocene rhyolite may reflect a greater quantity of heat transferred to the crust since eruption of the first basalt 3.6 m.y. ago and the fortuitous tectonically induced tapping of the top of a magma reservoir at a relatively late moment in its evolution.

The presence of both the Monache and Templeton domes near the centers of relatively low circular areas of subdued topography about 8 km in diameter invites speculation that these depressions may reflect underlying plutons (Heiken, 1976). However, if the suggested deep crustal origin and rapid ascent of the Monache and Templeton magmas are correct, it is unlikely that such a direct genetic connection exists.

The youth and composition of the rhyolite of Long Canyon suggest that a significant amount of heat associated with the silicic reservoir that fed the dome may still be present. Should this be true, it is conceivable that a small geothermal system may exist, perhaps with fluid distribution and mobility controlled by fractures oriented in the same sense as Long Canyon.

ACKNOWLEDGMENTS

We are indebted to the staff of the Branch of Analytical Laboratories of the U.S. Geological Survey for chemical analyses, R. W. Kistler and A. C. Robinson for $^{87}Sr/^{86}Sr$ determinations, and G. B. Dalrymple for $^{40}Ar/^{39}Ar$ and K-Ar age data. S. H. Wood brought the Long Canyon rhyolite locality to our attention. J. N. Batchelder kindly examined inclusions in the Monache garnet and fayalite with a petrographic microscope equipped with a freezing stage. T. K. Kyser measured $\delta^{18}O$ for the Monache rhyolite. The manuscript was much improved by the suggestions of Wes Hildreth, C. A. Hopson, R. W. Kistler, B. D. Marsh, and an anonymous reviewer.

REFERENCES

Albarede, F., and Bottinga, Y., 1972, Kinetic disequilibrium in trace-element partitioning between phenocrysts and host lava: Geochim. et Cosmochim. Acta, v. 36, p. 141-156.

Arth, J. G., 1976, Behavior of trace elements during magmatic processes — a summary of theoretical models and their applications: U.S. Geol. Survey Jour. Research, v. 4, p. 41-47.

Babcock, J. W., 1975, Volcanic rocks in the Coso Mountains, California: Geol. Soc. America Abs. with Programs, v. 7, no. 3, p. 291-292.

Babcock, J. W., and Wise, W. S., 1973, Petrology of contemporaneous Quaternary basalt and rhyolite in the Coso Mountains, California: Geol. Soc. America Abs. with Programs, v. 5, no. 1, p. 6.

Bacon, C. R., and Duffield, W. A., 1976, Phenocryst mineralogy of Pleistocene rhyolites and heat content of the Coso Range geothermal system, California: Geol. Soc. America Abs. with Programs, v. 8, no. 6, p. 761-762.

Bacon, C. R., Duffield, W. A., and Nakamura, K., 1980, Distribution of Quaternary rhyolite domes of the Coso Range, California: implications for extent of the geothermal anomaly: Jour. Geophys. Research, v. 85, p. 2425-2433.

Birch, W. D., and Gleadow, A. J. W., 1974, The genesis of garnet and cordierite in acid volcanic rocks: evidence from the Cerberean Cauldron, Central Victoria, Australia: Contr. Mineralogy Petrology, v. 45, p. 1-13.

Brousse, R., Bizourard, H., and Salat, J., 1972, Garnets from Slovakian andesites and rhyolites. The origin of garnets from the andesite series: Contr. Mineralogy Petrology, v. 35, p. 201-213.

Buddington, A. F., and Lindsley, D. H., 1964, Iron-titanium oxide minerals and synthetic equivalents: Jour. Petrology, v. 5, p. 310-357.

Carmichael, I. S. E., 1967, The iron-titanium oxides of salic volcanic rocks and their associated ferromagnesian silicates: Contr. Mineralogy Petrology, v. 14, p. 36-64.

Cox, A., and Dalrymple, G. B., 1967, Statistical analysis of geomagnetic reversal data and the precision of potassium-argon dating: Jour. Geophys. Research, v. 72, p. 2603-2614.

Crough, S. T., and Thompson, G. A., 1977, Upper mantle origin of Sierra Nevada uplift: Geology, v. 5, p. 396-399.

Dalrymple, G. B., 1963, Potassium-argon dates of some Cenozoic volcanic rocks in the Sierra Nevada, California: Geol. Soc. America Bull., v. 74, p. 379-390.

Dodge, F. C. W., 1972, Trace-element contents of some plutonic rocks of the Sierra Nevada batholith: U.S. Geol. Survey Bull. 1314-F, 13 p.

Donaldson, C. H., 1976, An experimental investigation of olivine morphology: Contr. Mineralogy Petrology, v. 57, p. 187-213.

Duffield, W. A., Bacon, C. R., and Dalrymple, G. B., 1980, Late Cenozoic volcanism, geochronology, and structure of the Coso Range, Inyo County, California: Jour. Geophys. Research, v. 85, p. 2381-2404.

Eugster, H. P., and Wones, D. R., 1962, Stability relations of the ferruginous biotite, annite: Jour. Petrology, v. 3, p. 82-125.

Evans, S. H., Jr., and Nash, W. P., 1975, Low-temperature rhyolite from the Roosevelt geothermal area, Utah: Geol. Soc. America Abs. with Programs, v. 7, no. 7, p. 1070.

Ferry, J. M., and Spear, F. S., 1978, Experimental calibration of the partitioning of Fe and Mg between biotite and garnet: Contr. Mineralogy Petrology, v. 66, p. 113-117.

Fitton, J. G., 1972, The genetic significance of almandine–pyrope phenocrysts in the calc–alkaline Borrowdale volcanic group, northern England: Contr. Mineralogy Petrology, v. 36, p. 231-248.

Flood, R. H., and Shaw, S. E., 1977, Two "S-type" granite suites with low initial $^{87}Sr/^{86}Sr$ ratios from the New England batholith, Australia: Contr. Mineralogy Petrology, v. 61, p. 163-173.

Friedman, I., and Smith, R. L., 1955, The deuterium content of water in some volcanic glasses: Geochim. et Cosmochim. Acta, v. 15, p. 218-228.

Green, D. H., and Hibberson, W., 1970, The instability of plagioclase in peridotite at high pressure: Lithos, v. 3, p. 209-221.

Green, T. H., 1976, Experimental generation of cordierite- or garnet-bearing granitic liquids from a pelitic composition: Geology, v. 4, p. 85-88.

Green, T. H., and Ringwood, A. E., 1968, Origin of garnet phenocrysts in calc–alkaline rocks: Contr. Mineralogy Petrology, v. 18, p. 163-174.

———— 1972, Crystallization of garnet-bearing rhyodacite under high-pressure hydrous conditions: Geol. Soc. Australia Jour., v. 19, p. 203-212.

Heiken, G., 1976, Depressions surrounding volcanic fields: A reflection of underlying batholiths?: Geology, v. 4, p. 568-572.

Helz, R. T., 1976, Phase relations of basalts in their melting ranges at $P_{H_2O} = 5$ kb. Part II. Melt compositions: Jour. Petrology, v. 17, p. 139-193.

Hewitt, D. A., 1978, A redetermination of the fayalite–magnetite–quartz equilibrium between 650 and 850°C: Am. Jour. Sci., v. 278, p. 715-724.

Hildreth, E. W., ms, 1977, The magma chamber of the Bishop Tuff: Gradients in temperature, pressure, and composition: Ph.D. thesis, Univ. California, Berkeley, Calif., 328 p.

Hildreth, W., 1979, The Bishop Tuff: evidence for the origin of compositional zonation in silicic magma chambers, *in* Chapin, C. E., and Elston, W. E., eds., Ash-flow tuffs: Geol. Soc. America Spec. Paper 180, p. 43-75.

Holloway, J. R., 1976, Fluids in the evolution of granitic magmas: consequences of finite CO_2 solubility: Geol. Soc. America Bull., v. 87, p. 1513-1518.
Hsu, L. C., 1968, Selected phase relationships in the system Al–Mn–Fe–Si–O–H: a model for garnet equilibria: Jour. Petrology, v. 9, p. 40-83.
Ishihara, S., 1977, The magnetite-series and ilmenite-series granitic rocks: Mining Geology, v. 27, p. 293-305.
Jack, R. N., and Carmichael, I. S. E., 1968, The chemical fingerprinting of acid volcanic rocks: California Div. Mines Geology Spec. Rept. 100, p. 17-32.
Kano, H., and Yashima, R., 1976, Almandine–garnets of acid magmatic origin from Yamanogawa, Fukushima Prefecture and Kamitazawa, Yamagata Prefecture: Japanese Assoc. Mineralogists, Petrologists, and Econ. Geologists Jour., v. 71, p. 106-119.
Keesman, I., Matthes, S., Schreyer, W., and Siefert, F., 1971, Stability of almandine in the system FeO–(Fe_2O_3)–Al_2O_3–SiO_2–(H_2O) at elevated pressures: Contr. Mineralogy Petrology, v. 31, p. 132-144.
Kistler, R. W., and Peterman, Z. E., 1973, Variations in Sr, Rb, K, Na, and initial Sr^{87}/Sr^{86} in Mesozoic granitic rocks and intruded wall rocks in central California: Geol. Soc. America Bull., v. 84, p. 3489-3512.
Knopf, A., 1918, A geologic reconnaissance of the Inyo Range and the eastern slope of the Sierra Nevada, California: U.S. Geol. Survey Prof. Paper 110, 130 p.
Lachenbruch, A. H., 1978/79, Heat flow in the Basin and Range province and thermal effects of tectonic extension: Pure and Appl. Geophysics, v. 117, p. 34-50.
Lawson, A. C., 1904, The geomorphogeny of the upper Kern Basin: Univ. Calif. Pub., Dept. Geology Bull., v. 4, p. 291-376.
Leake, B. E., 1967, Zoned garnets from the Galway granite and its aplites: Earth Planetary Sci. Letters, v. 3, p. 311-316.
Lipman, P. W., 1971, Iron–titanium oxide phenocrysts in compositionally zoned ash-flow sheets from southern Nevada: Jour. Geology, v. 79, p. 438-456.
Lockwood, J. P., and Moore, J. G., 1979, Regional extension of the Sierra Nevada, California, on conjugate microfault sets: Jour. Geophys. Research, v. 84, p. 6041-6049.
Maaløe, S., and Wyllie, P. J., 1975, Water content of a granite magma deduced from the sequence of crystallization determined experimentally with water-undersaturated conditions: Contr. Mineralogy Petrology, v. 52, p. 175-191.
Masuda, A., Nakamura, N., and Tanaka, T., 1973, Fine structures of mutually normalized rare-earth patterns of chondrites: Geochim. et Cosmochim. Acta, v. 37, p. 239-248.
Matthews, R. A., and Burnett, J. L., 1965, Geologic map of California, Fresno Sheet: California Div. Mines Geology, scale 1:250,000.
Mayo, E. B., 1947, Structure plan of the southern Sierra Nevada, California: Geol. Soc. America Bull., v. 58, p. 495-504.
Moore, J. G., and du Bray, E., 1978, Mapped offset of the right-lateral Kern Canyon fault, southern Sierra Nevada, California: Geology, v. 6, p. 205-208.
Nakamura, K., 1977, Volcanoes as possible indicators of tectonic stress orientation: Jour. Volcanology Geothermal Research, v. 2, p. 1-16.
Naney, M. T., ms, 1977, Phase equilibria and crystallization in iron- and magnesium-bearing grantic systems: Ph.D. thesis, Stanford Univ., 229 p.
Noble, D. C., Korringa, M. K., Hedge, C. E., and Riddle, G. O., 1972, Highly differentiated subalkaline rhyolite from Glass Mountain, Mono County, California: Geol. Soc. America Bull., v. 83, p. 1179-1184.
Oliver, H. W., and Robbins, S. L., 1979, Bouguer gravity map of California, Fresno Sheet: California Div. Mines Geology, scale 1:250,000.
Oliver, R. L., 1956, The origin of garnets in the Borrowdale volcanic series and associated rocks, English Lake District: Geol. Mag., v. 93, p. 121-139.
Reid, M. J., Gancarz, A. J., and Albee, A. L., 1973, Constrained least-squares analysis of petrologic problems with an application to lunar sample 12040: Earth Planetary Sci. Letters, v. 17, p. 433-445.
Robie, R. A., Hemingway, B. S., and Fisher, J. R., 1978, Thermodynamic properties of minerals and related substances at 298.15k and 1 bar (10^5 pascals) pressure and at higher temperatures: U.S. Geol. Survey Bull. 1452, 456 p.
Ross, C. S., and Smith, R. L., 1955, Water and other volatiles in volcanic glasses: Am. Mineralogist, v. 40, p. 1071-1089.
Shapiro, L., 1975, Rapid analysis of silicate, carbonate, and phosphate rocks — revised edition: U.S. Geol. Survey Bull. 1401, 76 p.
Shaw, D. M., 1970, Trace element fractionation during anatexis: Geochim. et Cosmochim. Acta., v. 34, p. 237-243.

Shaw, H. R., Smith, R. L., and Hildreth, E. W., 1976, Thermogravitational mechanisms for chemical variations in zoned magma chambers: Geol. Soc. America Abs. with Programs, v. 8, no. 6, p. 1102.

Shmulovich, K. I., and Shmonov, V. M., 1975, Fugacity coefficients of CO_2 from 1.0132 to 10000 bar and from 450° to 1300°K: Geokhimia, v. 4, p. 551-555.

Sibley, D. F., Vogel, T. A., Walker, B. M., and Byerly, G., 1976, The origin of oscillatory zoning in plagioclase: a diffusion and growth controlled model: Am. Jour. Sci., v. 276, p. 275-284.

Smith, R. L., 1979, Ash-flow magmatism, *in* Chapin, C. E., and Elston, W. E., eds., Ash-flow tuffs: Geol. Soc. America Spec. Paper 180, p. 5-27.

Stormer, J. C., Jr., 1975, A practical two-feldspar geothermometer: Am. Mineralogist, v. 60, p. 667-674.

Vennum, W. R., and Meyer, C. E., 1979, Plutonic garnets from the Werner batholith, Lassiter Coast, Antarctic Peninsula: Am. Mineralogist, v. 64, p. 268-273.

Walter, A. W., and Weaver, C. S., 1980, Seismicity of the Coso Range, California: Jour. Geophys. Research, v. 85, p. 2441-2458.

Webb, R. W., 1946, Geomorphology of the middle Kern River basin, southern Sierra Nevada, California: Geol. Soc. America Bull., v. 57, p. 355-382.

———— 1950, Volcanic geology of Toowa Valley, southern Sierra Nevada, California: Geol. Soc. America Bull., v. 61, p. 349-357.

White, A. J. R., and Chappell, B. W., 1977, Ultrametamorphism and granitoid genesis: Tectonophysics, v. 43, p. 7-22.

Wood, B. J., 1975, The influence of pressure, temperature and bulk composition on the appearance of garnet in orthogneisses — an example from South Harris, Scotland: Earth Planeary Sci. Letters, v. 26, p. 299-311.

Wood, C. P., 1974, Petrogenesis of garnet-bearing rhyolites from Canterbury, New Zealand: New Zealand Jour. Geology Geophysics, v. 17, p. 759-787.

Wood, S. H., 1977, Chronology of late Pleistocene and Holocene volcanics, Long Valley and Mono Basin geothermal areas, eastern California: U.S. Geol. Survey, Tech. Rept., contract 14-08-0001-15166, 55 p.

Wright, L., 1976, Late Cenozoic fault patterns and stress fields in the Great Basin and westward displacement of the Sierra Nevada block: Geology, v. 4, p. 489-494.

Wright, T. L., and Doherty, P. L., 1970, A linear programming and least squares computer method for solving petrologic mixing problems: Geol. Soc. America Bull., v. 81, p. 1995-2008.

Wyllie, P. J., 1977, Crustal anatexis: an experimental review: Tectonophysics, v. 43, p. 41-71.

Yakowitz, H., Myklebust, R. L., and Heinrich, K. F. J., 1973, FRAME: an on-line correction procedure for quantitative electron probe analysis: Natl. Bur. Standards Tech. Note 796, 46 p.

Zeck, H. P., 1970, An erupted migmatite from Cerro del Hoyazo, SE Spain: Contr. Mineralogy Petrology, v. 26, p. 225-246.